Abstract

BLAIR, THOMAS CORWIN. Nanoscale Investigation of Degradation Effects in Lead Zirconate Titanate by Piezoresponse Force Microscopy. (Under the direction of Alexei Gruverman and Angus I. Kingon)

This thesis reports results obtained by piezoresponse force microscopy (PFM) on the nanoscale mechanisms of imprint and fatigue, two of the most important degradation effects in ferroelectric materials. Imprint is the preference of a ferroelectric material for one polarization state over another. Fatigue is the loss of polarization due to repeated switching.

Imprint was investigated in three PZT films with thicknesses of 100, 300, and 500 nm. It was found that the imprint was most severe in the thinnest sample. This was attributed to the increasing dominance of interface effects in the thin sample. Furthermore, it was found that the presence of top electrodes moderated the imprint. This was explained by top electrode leading to a symmetric distribution of trapped space charge, as opposed to the asymmetric distribution when only the bottom electrode is present.

Fatigue was investigated in bulk ceramic PZT samples cycled to three different fatigue states (virgin, semifatigued, and fatigued) and then polished at an angle such that a range of thicknesses in the sample were available to be studied. It was found that the fatigued samples exhibited different domain structures. Backswitching occurred in the thick regions of the fatigued sample, but did not occur at any thickness in the virgin sample. This was explained by the cascaded backswitching model, positing that charged defects agglomerating at grain boundaries and provoking backswitching in all grains above it.

NANOSCALE INVESTIGATION OF DEGRADATION EFFECTS IN LEAD ZIRCONATE TITANATE BY PIEZORESPONSE FORCE MICROSCOPY

by

THOMAS CORWIN BLAIR

Submitted to the Graduate Faculty of
North Carolina State University
in partial fulfillment of the
requirements for the Degree of
Master of Science

MATERIALS SCIENCE AND ENGINEERING

Raleigh

2005

APPROVED BY:

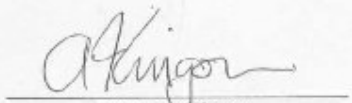

Angus I. Kingon
Chair of Advisory Committee

Alexei Gruverman
Co-Chair of Advisory Committee

Robert J. Nemanich

Biography

Thomas Corwin Blair was born in 1981 in Fairfax County, Virginia. He grew up in Dayton, Ohio, with his parents, John and Joyce, and his brothers, Nathaniel and Matthew. He attended Walter E. Stebbins High School.

Tom went on to Miami University (in Ohio, not Florida) in 1999 where he earned a B.S. in Engineering Physics and developed an interest in materials physics, especially in semiconductors and other electronic materials.

Finally, in 2003 he moved to Raleigh to study Materials Science and Engineering at North Carolina State University, where he worked with Dr. Gruverman, Dr. Kingon, and Dr. Nemanich on the characterization of ferroelectric materials

Acknowledgements

I had lots of help from lots of people during my time here in Raleigh. My thanks go to:

My advisors: Prof. Alexei Gruverman, Prof. Angus Kingon, Prof. Robert Nemanich; and also Dr. Brian Rodriguez. Their knowledge and resources was absolutely invaluable; without their help, my work here would have amounted to nothing.

My labmates in the AFM room: Nina Balke, Jacquie Hanson, Brian Rodriguez, John Waldrep, and Dong Wu. They made our lab a fun and productive place to work, and I'll never forget their friendship. They all helped in ways too numerous too mention, but I'll mention in particular John's help designing the summing circuit described in the introduction and Nina's collaboration with me on every aspect of the fatigue chapter of this thesis.

All the members of the Surface Science Lab. I wish every grad student could be lucky enough to work in a research group like ours. They taught me how to use equipment, answered my questions, and were a great group of people to work and hang out with. They are: my aforementioned labmates, Eugene Bryan, James Burnette, Jiyoung Choung, Charlie Fulton, Jacob Garguilo, Benjamin Gilbert, Franz Koeck, Wendy Kong, James Perkins, Sarah Reising, Joshua Smith, Anderson Sunda-Meya, Yingjie Tang, Joseph Tedesco, Jennifer Walter, Leigh Winfrey, and Matt Zeman.

Jon-Paul Maria and his research group, for their resources, knowledge, and helpfulness. In particular, I'm grateful to Jon Ihlefeld and Spalding Craft, for sputtering electrodes; Brian Laughlin, for teaching me how to polish samples; and Dr. Taeyun Kim, for helping set up a ferroelectric testing device.

The Kingon group (particularly Dr. Dan Lichtenwalner and Dr. Sudarsan Srinivasan) for useful discussions and help with annealing samples.

The National Science Foundation and North Carolina State University, for funding my research and putting food on my table.

And, finally, my family and friends, for reasons I can't even begin to go into here.

Table of Contents

List of Figures

Chapter 1: Introduction

1.1 Motivation

Ferroelectric materials have long had important hi-tech applications. As the field of nanoelectronics has become more and more pervasive, the effort to build smaller, faster devices has pushed ferroelectrics to an even more prominent position. In particular, the appeal of ferroelectric memory devices, especially non-volatile ferroelectric random access memory (NVFRAM), has driven interest and funding for ferroelectrics. The potential of ferroelectrics to serve as memory devices has been known since the mid-1950s [1]. Now, 50 years later, such memory devices are in limited production through a number of large companies, such as Samsung, Fujitsu, Ramtron, and Toshiba. Ferroelectric memory promises to revolutionize computer architectures because of their speed, density, and non-volatility. However, degradation effects have been a major obstacle to its widespread adoption.

The nanoscale applications of ferroelectrics demand their nanoscale characterization. How do degradation effects scale with size? What clues can nanoscale characterization provide to show us their mechanisms? This thesis attempts to address these questions by providing an overview of our understanding of degradation effects and presenting results obtained by atomic force microscopy (AFM), and, more specifically, by piezoresponse force microscopy (PFM).

1.2 Ferroelectricity

Ferroelectricity is characterized by a spontaneous polarization that can be switched through the application of an electric field. Ferroelectric materials are a subset of piezoelectric materials.

Piezoelectric materials become electrically polarized when they are strained. This property arises from the symmetry characteristics of certain crystal classes. 11 of the 32 crystal classes have a center of symmetry and cannot have polar properties. The remaining 21 classes, however, have no center of symmetry and, with one exception (class *432*), have polar properties making them piezoelectric.

The absence of symmetry in piezoelectric materials results in microscopic dipoles caused by the displacement between the positive and negative charges in the unit cell. 10 of the 20 piezoelectric crystal classes have no net polarization, as the microscopic dipoles sum to zero except when the crystal is strained. The remaining 10 piezoelectric classes exhibit a *spontaneous* polarization even when the crystal is unstrained. These crystals are referred to as pyroelectric.

Pyroelectrics can be further divided into two groups – those with a *switchable* spontaneous polarization, and those without. Which of these two groups a pyroelectric material belongs to can only be determined experimentally.

Ferroelectrics are defined as pyroelectric materials with a switchable polarization [Figure 1].

Ferroelectrics have a material-dependent Curie temperature above which the material ceases to exhibit ferroelectric behavior, and instead becomes paraelectric. In the paraelectric phase the material has no spontaneous polarization. The transition between

the paraelectric and ferroelectric phase is accompanied by a change in the unit cell's structure. In the case of perovskite ferroelectrics such as lead zirconate titanate, the focus of this thesis, the unit cell distorts from a cubic unit cell in the paraelectric phase to an asymmetric unit cell.

1.2.1 Lead Zirconate Titanate

One well-known family of ferroelectric materials is composed of the solid solution of $PbZrO_3$ and $PbTiO_3$, commonly called "PZT." In the paraelectric phase, PZT has a cubic perovskite structure [Figure 2]. Below the Curie temperature, in the ferroelectric phase, it distorts slightly to an orthorhombic, rhombohedral, or tetragonal unit cell depending on the ratio of zirconium to titanium in the solution [Figure 3] .

PZT has several desirable characteristics both as an element in FRAM and in bulk ceramic applications. First, it has a high switched polarization value (40-80 C/m^2), and second, its crystallization temperature is low (550-600˚C) [2]. The low crystallization temperature makes integration with silicon technologies easier, and the high polarization makes detection of the polarization state more reliable.

1.2.3 Ferroelectric Domains

As was mentioned earlier, a requisite characteristic of ferroelectric crystals is that their polarization direction is switchable. In tetragonal PZT, for example, the central ion can be displaced toward any one of the six faces formed by the oxygen atoms. Adjacent unit cells tend to be polarized in the same direction, forming regions called ferroelectric domains. Thus PZT has six possible domain states. Domains are separated by thin (~1-

10 lattice constants) domain walls [2]. Recent first-principles linear-response studies of the structural energetics of the cubic perovskite structure shows that the ultimate limit on the lateral domain size of perpendicularly polarized ferroelectric films is two lattice constants [3].

Domain walls can be described by the angle between the polarization directions on either side. Thus, again in tetragonal PZT, domain walls can be either 180˚ or non-180˚. 180˚ walls separate antiparallel domains. 90˚ walls separate perpendicular domains. 180˚ and 90˚ domains are sometimes referred to as *a* and *c* domains, respectively, and perpendicular walls are referred to as *a*-*c* domain walls. Both cases are illustrated schematically in Figure 4. Because the unit cells of *a* and *c* domains distort in different directions, their formation affects the surface topography, corrugating the surface (Figure 4).

1.2.4 Thin Films and Bulk Ceramics

Since the 1980s, it has been possible to fabricate ferroelectrics in the form of thin films. Before that, ferroelectrics were available only in the forms of bulk ceramics and single crystals. Ferroelectric bulk ceramics are manufactured through a multi-step process involving mixing, calcining, milling, and sintering. Ferroelectric thin films are fabricated by physical vapor deposition, chemical vapor deposition, or chemical solution deposition.

Thin films tend to have smaller grains and lower d_{33} values than bulk ceramics [4]. The lower d_{33} value in thin films is attributed to its restricted domain wall motion. Thin films are also subject to biaxial stress, which can alter domain structure and switching [5].

Bulk ceramics have a number of important applications. They are used as actuators (devices allowing very small, precise amounts of displacement), and transducers (devices converting electrical energy into mechanical energy). The former category includes precision x-y stages such as those used in AFMs, and the latter includes a variety of important devices, from SONAR to medical ultrasounds.

Thin films have attracted the most attention recently for their applications in ferroelectric memory devices, especially FRAM. The high-dielectric properties of ferroelectrics have also generated interest in incorporating them into DRAM capacitors, replacing SiO_2 as the dielectric.

1.3 Atomic Force Microscopy

The atomic force microscope (AFM) was invented in 1986 by Binnig, Quate, and Gerber [6]. While it was originally intended to measure the topography of surfaces, it has proven to be a versatile tool, allowing for, among other things, nanometer-scale measurements of electronic properties of materials. The details of AFM are the subject of numerous books [7-10].

There are three main components to an AFM: a scanner, cantilever, and detector. As the scanner moves sample or the cantilever, it senses forces from the sample, which it reports to the detector. The scanner is a ceramic piezotube that scans according to a voltage applied by the controlling computer. The cantilever is typically a beam composed of silicon or silicon nitride, having a sharp tip with a radius of ~20 nm on one side, and a reflective backside. A laser bounces off the cantilever backside to the

position-sensitive photodetector (PSPD). The PSPD is composed of four photodiodes, and thus can sense minute tip deflections [Figure 5].

Two AFMs were used in this thesis. The primary AFM was a ThermoMicroscopes CP-Research, which scans the sample while holding the tip in one place. The secondary AFM was a Park Scientific Instruments M5, which scans the tip. The CP-Research has higher resolution and is less noisy than the M5. However, the M5 was designed for larger samples, and is useful when one measures large samples or uses external probes (see PFM Experimental Setup). The M5 also has the advantage of superior optics, allowing one to easily locate microscopic features.

AFMs can be operated in contact mode or non-contact mode. In contact mode, the tip-sample distance is small enough to be in the repulsive regime of atomic interactions. The tip is deflected with some constant amount of force. As the force exerted on the tip changes by some small amount, the scanner reacts, adjusting the tip-sample separation to return the tip to its original deflection. The topographic image is then derived by compiling the voltages applied to the scanner to adjust the tip-sample separation. All images included in this thesis were taken in contact mode.

In non-contact mode, the tip-sample distance is kept in the attractive regime (~1-10 nm). As the force the tip changes, the resonant frequency of the cantilever will change. The AFM then adjusts the tip-sample separation in order to maintain the cantilever's original resonant frequency. As with contact mode, the topographic image is generated by compiling the adjustments in the tip-sample separation. Non-contact imaging is most useful when imaging surfaces with loosely-bound particles that can easily be moved about the surface, or very soft surfaces that could be damaged by an AFM tip.

1.4 Piezoresponse Force Microscopy

PFM has in the last decade been established as one of the principle tools for characterizing ferroelectrics at the nanometer scale. PFM images are derived from the detection of bias-induced sample deformation due to the converse piezoelectric effect. The piezoelectric response of the sample is the first harmonic component of the bias-induced tip deflection,

$$d = d_0 + R\cos(\omega t + \theta). \quad (1)$$

θ is the phase of the electromechanical response, and R is the amplitude. c^+ and c^- domains will have two possible phase states – +90° (in phase with the applied tip bias), and -90° (out of phase with the tip bias). *a* domains will have a phase of 0° [Figure 6].

The amplitude of the experimentally determined piezoresponse is composed of more than just the electromechanical contribution. Also included are the electrostatic contribution, and the non-local contribution due to capacitive cantilever-surface interactions [11-13]. These effects can shift the PFM phase and distort the amplitude, and have been addressed by Kalinin *et al.*[14].

We operate under the convention that a domain is positive if its polarization vector is oriented toward the substrate. This means that domains that have been switched by application of a positive voltage are positive and those that have been switched by a negative voltage are negative (Figure 6).

1.4.1 PFM Experimental Setup

PFM setups require that a voltage be applied between a tip and a back electrode. The applied AC voltage (referred to as the driving or modulation voltage) creates an alternating electric field causing the sample to expand and contract at the same frequency due to the converse piezoelectric effect.

A lock-in technique is used to detect the sample expansion and contraction, and this mechanical oscillation is then compared to the driving voltage to determine whether they are in phase or out of phase. The tip is rastered across the sample surface and the phase relative to the amplitude is measured at each point. These points are combined to form the PFM phase image.

Also using a lock-in technique, the amplitude of the bias-induced mechanical oscillation of the sample can be determined. Large oscillations are indicative of a high piezoelectric constant, appearing white in PFM images.

The driving voltage can be applied to either the tip or to the sample bottom electrode. Furthermore, the top electrode can be either the tip itself or a larger metal electrode deposited on the surface.

Using only the tip as the top electrode results in an inhomogeneous field applied to the underlying material, making accurate piezoelectric measurements problematic. First of all, calculations modeling the tip-generated electric field must be performed in order to eliminate tip-sample interactions. Second, since the field is applied in a localized region, switching can be inhibited by nearby, non-stimulated regions. On the other hand, using the tip as the top electrode allows for the direct study of individual domains and

how they grow and switch. Measurements performed in this manner are referred to as "bare surface" measurements.

Using a top electrode deposited on the sample results the underlying material experiencing a homogeneous electric field, as all domains feel the same force. For small capacitors, the electrode is driven by the tip itself. For larger capacitors, an external probe held at the same potential as the tip is used. This arrangement allows for quantitative measurements, as there are no tip-sample interactions or mechanical constraints from nearby regions. Individual domains can be observed with this setup. However, it has the disadvantage that individual domains cannot be studied as closely as the bare surface measurements allow, as the electric field will be applied to all domains underneath the electrode instead of only those underneath the tip.

1.4.2 PFM Electronics

As the AFM tip is rastered across the sample, the phase (θ) and amplitude (R) of the piezoresponse should be measured simultaneously. To this end, we employ a dual-phase lock-in amplifier (Stanford Research Systems SR830). The internal function generator of the lock-in amplifier provides the ac driving voltage.

The phase component of the piezoresponse is measured from the Aux 4 output of the AFM. The amplitude component is measured from the Raw A1M3 output of Veeco's Extended Signal Access Module.

The dc signal is provided by a Keithley 236 Source Measure Unit. In cases where both the ac and dc signal should be applied simultaneously, the signals are routed to a home-built summing circuit that can operate at voltages up to +/-150 V (Figure 7).

1.4.3 Sources of Error

As with most nanoscale measurements, there are numerous possibilities for error in AFM measurements, both topographic and electrical. The two most common sources of error in topographic measurements are tip imaging and drift. Tip imaging occurs when a feature on the tip is larger than the surface features. It usually manifests itself as a repeated shape in the topographic image [Figure 8]. Drift occurs when the scanner, sample, or tip moves in a way additional to the normal scanning motion. It can be divided into two cases – scanner drift, in which the piezotube itself has a net movement beyond its scanning, and sample drift, in which the sample moves. Scanner drift can usually be eliminated by allowing the system to scan for about 10 minutes before taking further measurements. Sample drift is usually caused by improperly fixing the sample—for example, by using double sided tape—and can be solved by fixing the sample with silver paint or correctional fluid (like WhiteOut). Other scanner-induced errors such as creep, aging, and cross-coupling are discussed elsewhere [10].

There are several sources of error in piezoelectric measurements in the AFM. One is a loss of electrical contact from the tip. This can be caused by, in the case of metal-coated tips, the coating wearing off, or, in the case of doped silicon tips, an oxide layer forming at the tip surface.

As was addressed in the Principles of PFM section of this thesis, the cantilever's ac bias provokes more than just a piezoelectric response. It also induces electrostrictive and electrostatic interactions [16].

If the ac driving voltage applied to the tip exceeds the sample's coercive voltage, PFM imaging becomes destructive and can inadvertently switch domains. Because there is a possibility that even low voltages can switch domains during imaging, it is best to keep the driving voltage as low as possible while still obtaining quality images – around 25% of the coercive voltage is typical.

1.5 Polarization Fatigue

Polarization fatigue is the loss of polarization due to repeated switching [Figure 9]. It is a primary degradation effect in ferroelectrics, and is problematic for memory devices because their sensors rely on high polarization values for detection of the polarization state. It is named in analogy to mechanical fatigue.

The onset and extent of fatigue depends on both the ferroelectric and the capacitor materials. For example, PZT with platinum electrodes (Pt/ PZT/ Pt), experiences strong fatigue, losing about 50% of its polarization after 10^{10} switching cycles [2]. Some oxide electrodes, such as IrO_2, have high endurance, retaining nearly its original polarization after as many as 10^{15} switching cycles. Fatigue has become less of a problem in recent years with the introduction of oxide electrodes. Furthermore, some ferroelectrics such as SBT, exhibit very little fatigue behavior. However, fatigue is still not well-understood, and, in addition to being scientifically interesting, better knowledge of it could lead to faster, more reliable devices with longer lifetimes.

1.5.1 Fatigue Mechanisms

Tagantsev laid out three families of possible fatigue mechanisms in his 2001 review paper:

1) reduction of the effective electrode area,
2) reduction of the effective field, and
3) modification of the switching process [16].

These mechanisms are by no means mutually exclusive, and it is possible that each of them plays a role in fatigue, and that different mechanisms dominate in thin films and bulk ceramics.

Effective electrode area reduction

The effective electrode area can be reduced through burning, delamination, and cracking under the top electrode. These processes will result in a reduction of the number of domains under the top electrode. Thus, all polarization-related aspects of the capacitor, as well as the conduction and small-signal dielectric constant, should scale by the same factor. Johnson *et al*. demonstrated this mechanism by delaminating an electrode and measuring the conduction, dielectric constant, and remanent polarization [17]. This mechanism is always a possible source of fatigue, but it is also believed to be controllable through improved processing techniques.

Effective field reduction

The effective field under the top electrode will be reduced if a non-switching layer forms directly underneath it. This case is described by

$$E_f = E - \frac{d}{\varepsilon_d L} P,$$

Where L is the film thickness, d is the thickness of the non-switching layer, ε_d is the dielectric permittivity, and P is the polarization of the ferroelectric film [18-20]. Mathematical modeling shows that this mechanism manifests itself by a tilt of the hysteresis loop, leaving the coercive field either unchanged or slightly decreased [20].

Switching modification

To discuss the possible modifications of the switching process we must first discuss our model of the switching process. Polarization vectors grow from "seeds." In a ferroelectric with normal switching behavior, both positive and negative seeds exist, and the seed growth is uninhibited in either direction [Figure 10].

There are three sub-mechanisms of the switching modification mechanism – domain wall pinning, seed inhibition, and local imprint. *Domain wall pinning* supposes that domain walls are frozen in place by the interaction between charged defects on the domain walls and mobile charge carriers [21]. This mechanism requires that there are only seeds of one domain direction in the pinned domain [Figure 11]; otherwise switching would proceed normally.

The *seed inhibition* mechanism predicts that seeds are prevented from growing when they are in their embryonic state. At the electrode interfaces, where there is a high defect concentration, seeds in one direction are prevented from growing [Figure 12].

Finally, the *local imprint* mechanism posits that fatigue and imprint have a common cause at the microscopic scale [22]. Screening charges on the electrode migrate to the ferroelectric and become trapped there. Then interactions between them and the

polarization bound charge impede the domain wall motion and the nucleation of opposite domains [Figure 13]. The difference between imprint and fatigue occurs at the macroscopic scale – imprint implies that all or most regions are imprinted in the same direction, whereas fatigue implies a more or less even mixture of imprinted regions (i.e. if most individual domains are imprinted in the same direction, macroscopic imprint occurs, but if there is an even mix of imprint directions in individual domains, macroscopic fatigue occurs).

1.5.2 The role of defects

Except in the case of reduced electrode area, all of the above mechanisms rely on the creation of new defects or the redistribution of existing defects. There is a growing (albeit incomplete) consensus among researchers that the redistribution of oxygen vacancies is responsible for fatigue. Under this assumption, oxide electrodes draw the oxygen vacancies from the ferroelectric layer, explaining their high fatigue endurance [23,24]. This explanation is also appealing because oxygen vacancies are the most mobile ionic defects in PZT.

Another possible source of defects is electron injection. High energy electrons and holes can move from the electrode into the ferroelectric, creating space charge where the charge carriers stop, and other defects where the injected charges interact with the crystal. The electron injection could result in a number of fatigue mechanisms – the formation of a non-switching layer, the inhibition of oppositely polarized seeds, domain wall pinning, and local imprint. The improved fatigue behavior of oxide electrodes is

explained by the creation of a network of conducting grain boundaries near the interface, resulting in charge relaxation near the electrode [25].

1.6 Imprint

Imprint is the tendency of one polarization state to be more favorable than another. It is named after imprint in ducklings – after birth, they will on instinct follow the first creature they see.

Imprint in ferroelectrics, on the other hand, is an aging effect. It is widely accepted to be caused by an asymmetric distribution of trapped charges which screen the polarization state [26,27]. The polarization vector draws a space charge to compensate for the ferroelectric's polarization. Imprint occurs when the space charge forms, generating a fixed internal and interfacial field that makes the polarization switch more easily in one direction than in the other [Figure 14]. The mechanisms of imprint are described in detail in Chapter 2.

The mechanism by which these charges become trapped is believed to be related to charge injection. A low-dielectric, low polarization interfacial layer often forms between the electrode and ferroelectric layer [28, 29]. Charge injection can occur due to the high electric field this layer experiences in the poled state [29]. The injected charge is then captured in the interfacial layer.

Imprint manifests itself in a voltage shift of the hysteresis loop. It is also usually accompanied by a lower d33 value at one end [Figure 15]. The voltage shift can mean, especially at low operating voltages, a memory device may not switch when it is supposed to. In some cases imprint can lead to backswitching, the spontaneous

reorientation of polarization to its original state following a switch. These effects are examples of write failures.

Imprint is often accompanied by a decrease in the remanent polarization, which can also lead to write failures.

There are two ways to reduce imprint effects in ferroelectrics – from a materials perspective, by reducing the concentration of charged impurities, and, from an electrical engineering perspective, by applying a restore pulse about every million cycles [30].

1.7 References

1. Anderson, J.R., Electl Engr **71**, 916 (1952).
2. R. Waser, *Nanoelectronics and Information Technology* (WILEY-VCH GmbH & Co. KGaA, 2003.
3. J. Scott, Ferroelectrics **260**, 3065 (2001).
4. S. Trolier-McKinstry, P. Aungkavattana, F. Chu, J Lacey, J.-P. Maria, J. J. F. Shepard, T. Su, and F. Xu, *Ferroelectric Thin Films VI*, edited by R. E. Treece, R. E. Jones, C.M. Foster, S. B. Desu and I. K. Yoo (Boston, 1997), Vol. 493 p. 59.
5. S.B. Desu, *Materials Research Society*, edited by E. R. Myers and A. I. Kingon (San Francisco, 1990), Vol. 200, p. 199.
6. G. Binning, C. F. Quate, and C. Gerber, Phys. Rev. Lett. **56**, 930-933 (1986).
7. D. Sarid, Exploring Scanning Probe Microscopy with Mathematica (John Wiley & Sons, Inc., 1997).
8. D. Sarid, Scanning Force Microscopy with Applications to Electric, Magnetic and Atomic Forces (Oxford University Press, NY, 1991).
9. R. Wiesendanger, *Scanning Probe Microscopy and Spectroscopy Methods and Application* (Cambridge University Press, Cambridge 1994).
10. R. Howland and L. Benatar, *A Practical Guide to Scanning Force Microscopy* (Park Scientific Instruments, 1993).
11. Hong J. W., Noh K., H. Park S. I., Kwun S. I., and Kim Z. G., Rev Sci Instrum **70**, 1735 (1999).
12. Eng L. M., Guntherodt H. J., Schneider G. A., Kopke U. And Munoz-Saldana, J Appl Phy Lett **74**, 233 (1999).
13. Franke K., Huelz H., and Weihnacht M. Surf Sci **415**, 178-182.
14. Kalinin S. V. And Bonnell D. A., *Nanoscale Characterisation of Ferroelectric Materials*, edited by Alexe M. and Gruverman, A. (New York, 2004).
15.
16. Tagantsev A. K., Stolichnov I., Colla E. L., Setter N., J Appl Phys **90**, 1387.
17. D. J. Johnson, D. T. Amm, E. Griswold, K. Sreenivas, G. Yi, and M. Sayer, Mater Res Soc Symp Proc **200**, 289 (1990).
18. S. L. Miller, R. D. Nasby, J. R. Schwank, M. S. Rogers, and P. V. Dressendorfer, J appl Phys **68**, 6463 (1990).
19. C. J. Brennan, Ferroelectrics **132**, 245 (1992).
20. A. K. Tagantsev, M. Landivar, E. Colla, and N. Setter, J appl Phys **78**, 2623 (1995).
21. W. L. Warren, D. Dimos, B. A. Tuttle, G. E. Pike, R. W. Schwartz, P. J. Clew, and D. C. McIntyre, J Appl Phys **77**, 6695 (1995).
22. V. Y. Shur, E. L. Rumyantev, E. V. Nikolaeva, E. I. SHishkin, and I. E. Baturin, Abstract of the 6th International Symposium on Ferroic Domains and Mesoscopic Structures, Nanjing, China, May-June 2000, p. 81.
23. Yoo I. and Desu S., Phys Status Solidi A **133**, 565 (1992).
24. J. F. Scott, C. A P. D. Araujo, B. M. Melnick, L. D. McMillan, and R. Zuleeg, J appl Phys **70,** 382 (1991).
25. J. Cross, M. Fujiki, M. Tsukada, K. Matsuura, S. Otani, M. Tomotani, Y. Kataoka, Y. Kotaka, and Y. Goto, Integr Ferroelect **25**, 265 (1999).

26. R. R. Mehta, B. D. Silverman, and J. T. Jacobs, J Appl Phys **44**, 3379, (1973).
27. A. Gruverman and M. Tanaka, J Appl Phys **89**, 1836 (2001).
28. M. Grossmann, O. Lhose, D. Bolten, U. Boettger, and R. Waser, *Ferroelectric Thin Films X*, edited by S. R. Gilbert, S. Trolier-McKinstry, Y. Miyasaka, S. Streiffer, and D. Wouters, MRS Symposium Proceedings No. 688 (Pittsburgh 2002).
29. A. Tagantsev and I. Stolichnov, Appl Phys Lett **74**, 1326 (1999).
30. Scott J. F., *Ferroelectric Memories* (Springer, New York: 2000).

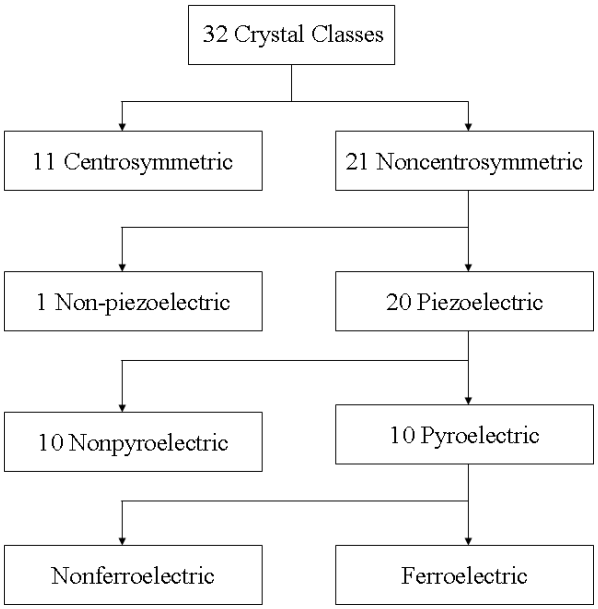

Figure 1.1: The division of the 32 crystal classes into noncentrosymmetric structures, piezoelectrics, pyroelectrics, and ferroelectrics.

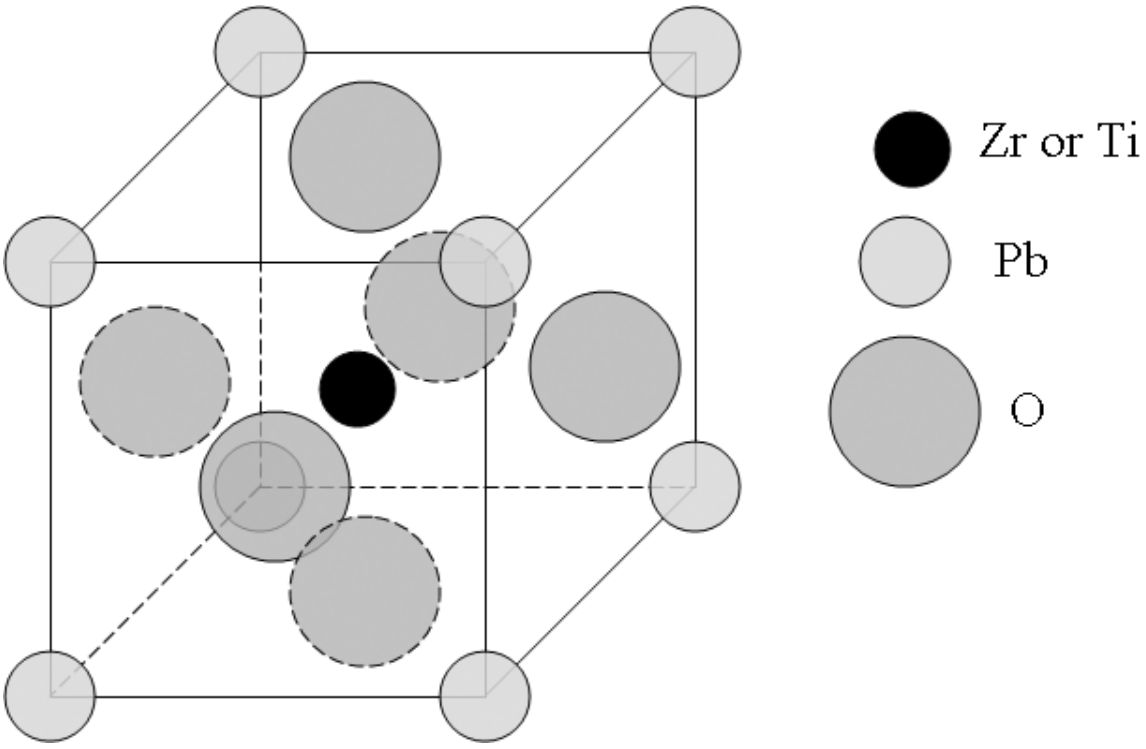

Figure 1.2: A lead zirconate titanate unit cell in the cubic (paraelectric) state.

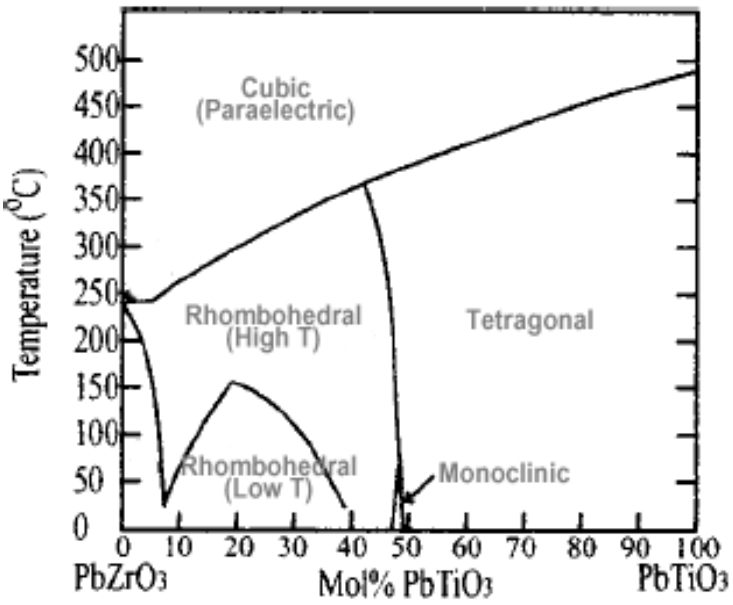

Figure 1.3: The sub-solidus phase diagram of PZT.

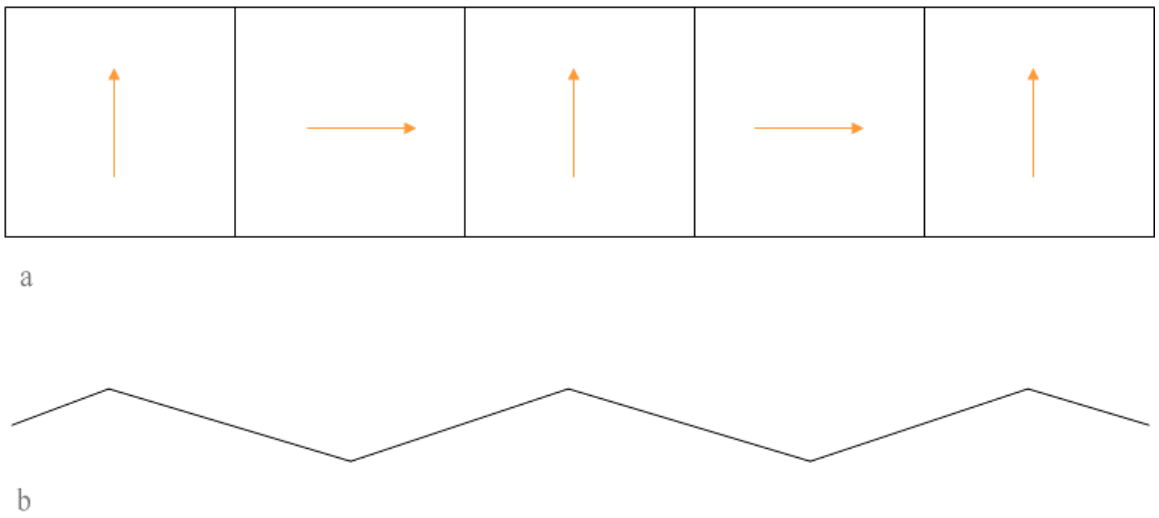

Figure 1.4: a) Schematic of *a*-*c* polarization vectors. b) Topographic corrugation due to *a*-*c* domains.

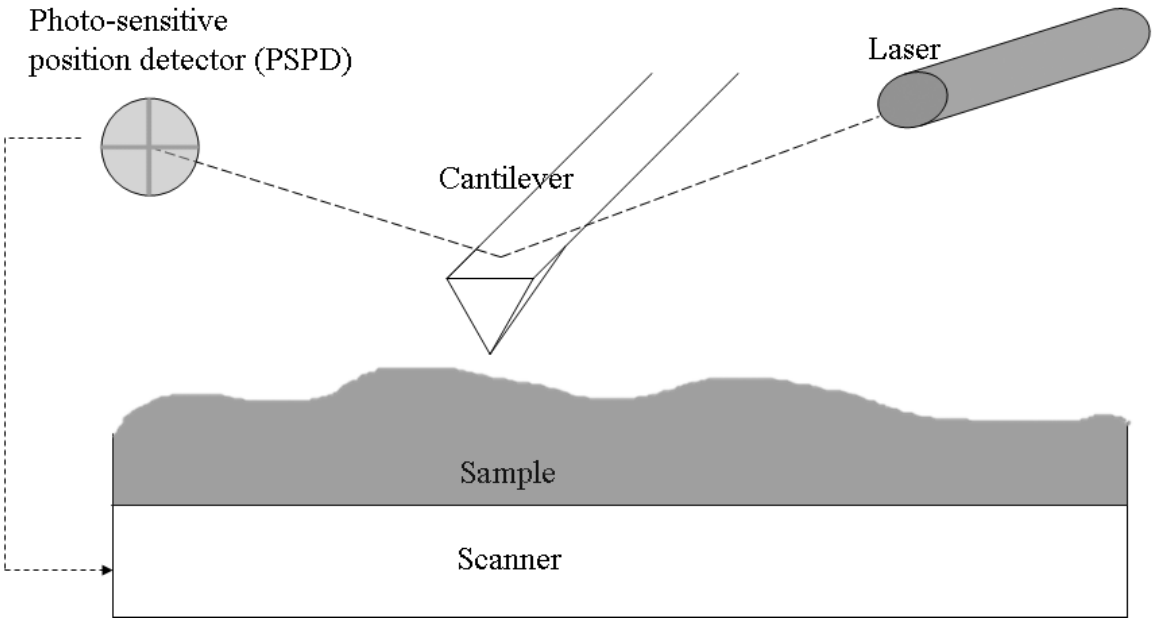

Figure 1.5: Schematic diagram of an atomic force microscope (AFM).

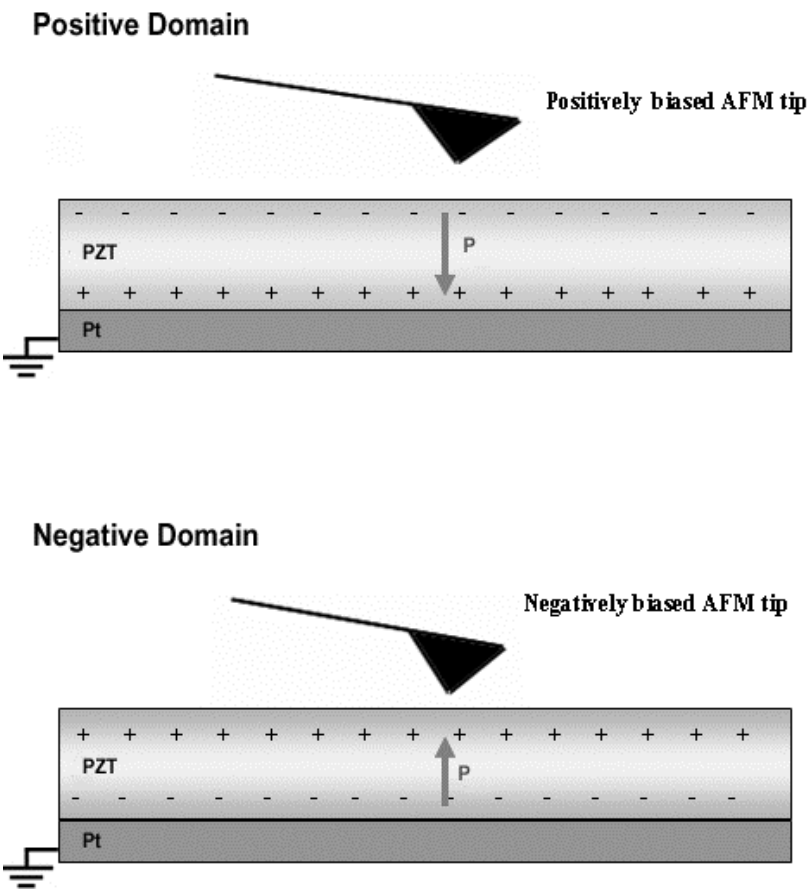

Figure 1.6: Ferroelectric polarization convention used in this thesis.

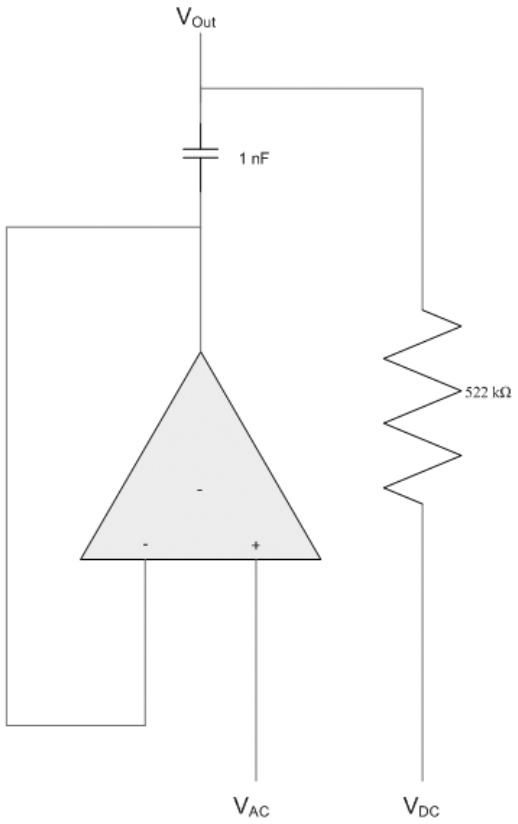

Figure 1.7: AC + DC summing circuit.

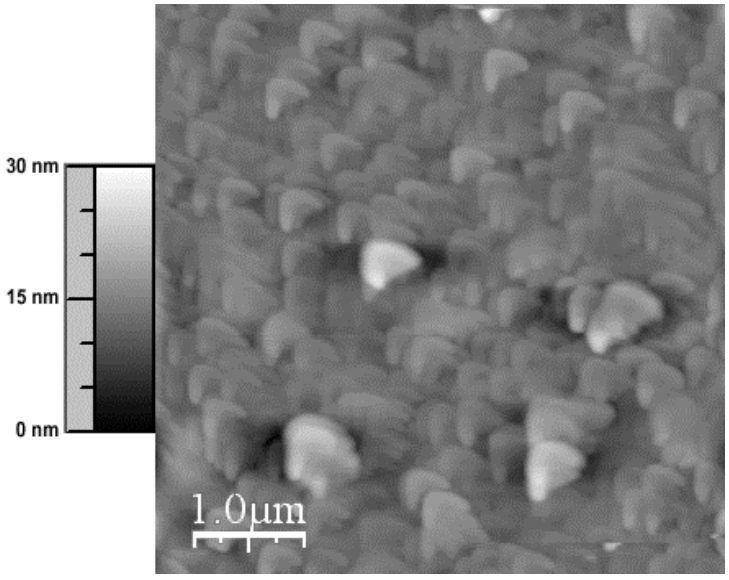

Figure 1.8: Example of repeated topographic features due to tip imaging (image courtesy of Dong Wu).

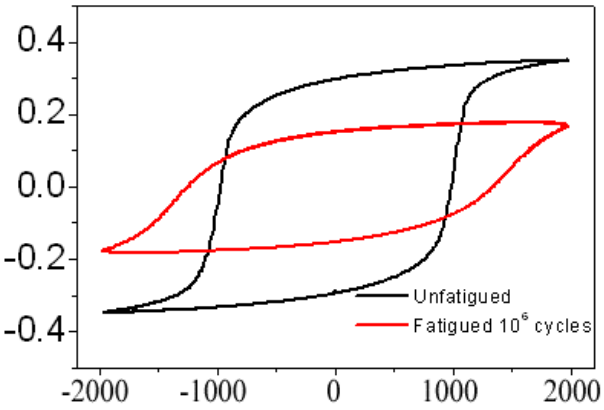

Figure 1.9: Virgin and fatigued polarization (C/m^2) vs. voltage (V) graphs.

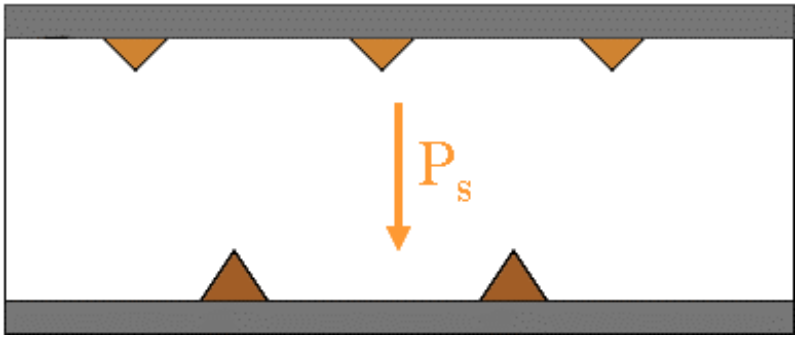

Figure 1.10: Polarization seeds in a normal ferroelectric material.

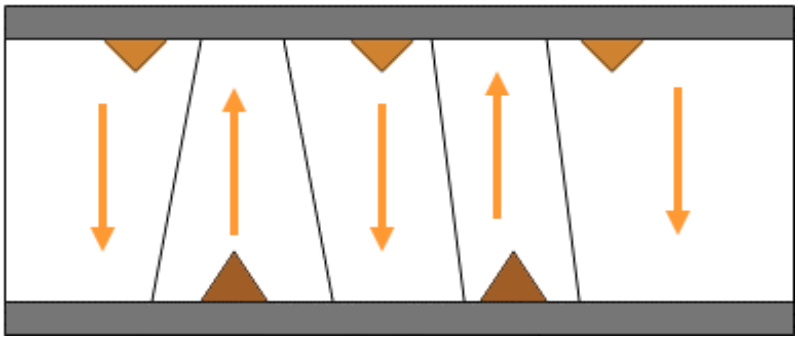

Figure 1.11 – Domain wall pinning.

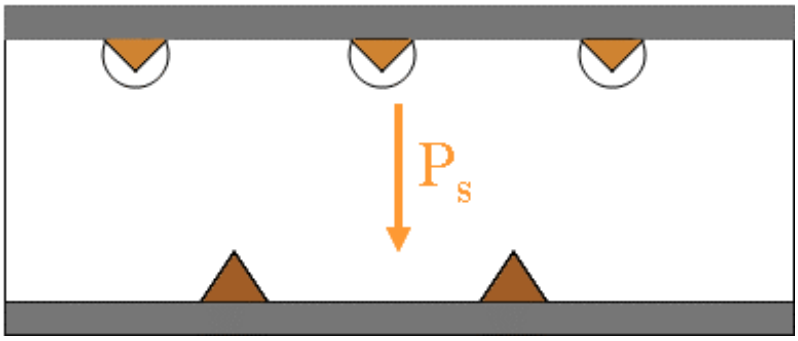

Figure 1.12 – Seed Inhibition.

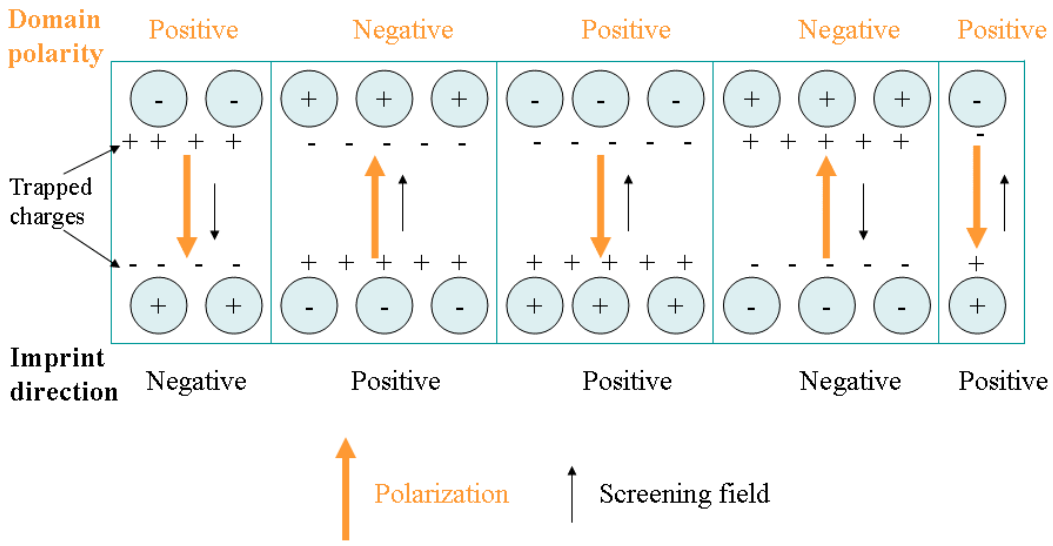

Figure 1.13 – Local Imprint.

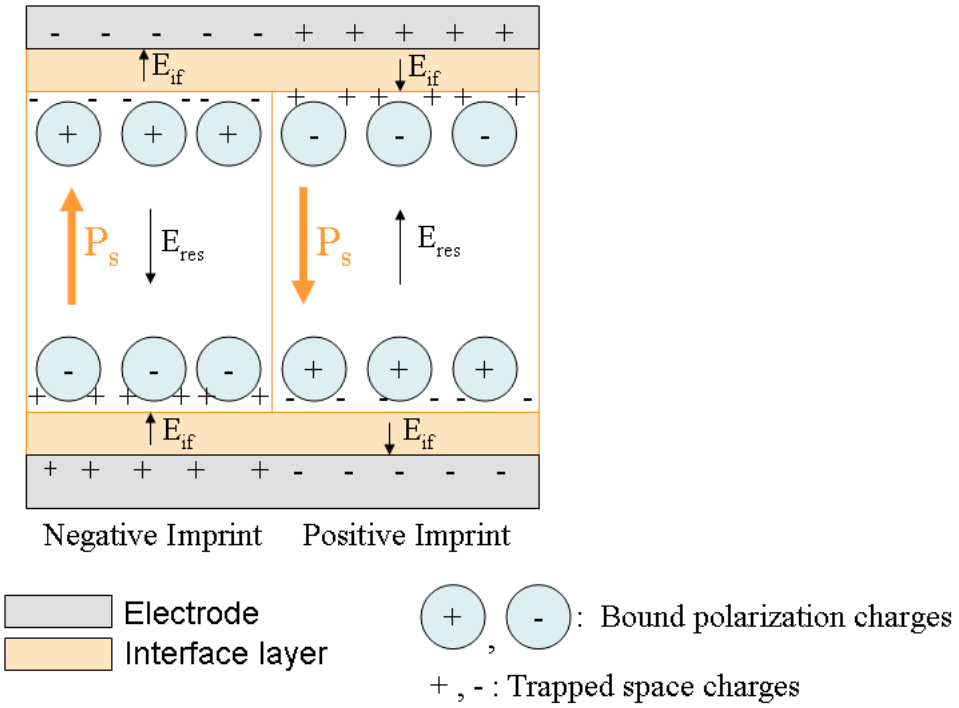

Figure 1.14 – Schematic of imprint caused by space charges.

Chapter 2: Size and Electrode Effects in PZT Thin Films

2.1 Introduction

As was discussed in the introduction, imprint is the preference of a ferroelectric material for one polarization state over another. It manifests itself by 1) a lateral shift of the hysteresis loop, and 2) backswitching to its preferred state. Imprint is thought to be caused by an asymmetric distribution of immobilized space charges in the ferroelectric.

Imprint is an impediment to the adoption of ferroelectric thin films in memory devices, as it can lead to both read and write failures [1]. The size scaling effects of this degradation mechanism are also of interest. In this set of experiments we sought to study the effects of capacitors and thickness on imprint and correlate these results to the nanoscale mechanisms of imprint.

The films investigated were tetragonal (30% zirconium, 70% titanium) PZT with thicknesses of 100, 300, and 500 nm. The structure of the capacitors was Pt/PZT/Pt. The films were provided by Inostek, Inc., a Korean-based manufacturer of PZT thin films.

2.2 Experiment

The samples were studied chiefly using piezoresponse force microscopy (PFM), detailed in the Chapter 1.4. To summarize, PFM is used to obtain a nanoscale map of a ferroelectric's domain structure [2,3]. An ac voltage is applied to the tip, inducing vibration in the film via the converse piezoelectric effect. The polarization direction is measured by detecting the phase difference between the driving voltage and the film vibration using a standard lock-in technique. The amplitude of the vibration, which is

proportional to the d_{33} piezoelectric coefficient, is also obtained. This technique allows for non-destructive imaging of the nanoscale domain structure.

Measurements were performed both on the bare surface of the thin film and on the top electrodes. The measurements on the top electrode were performed using an external probe held at the same potential as the PFM tip [4]. This procedure results in a homogeneous electric field applied to the ferroelectric while minimizing electrostatic interactions.

Domain switching was explored first by positioning the tip at a selected point on the sample and cycling the dc voltage while simultaneously applying the ac imaging voltage. In this manner phase and amplitude loops over a small area, limited by the tip radius, are obtained. These measurements were performed on both top electrodes and bare surfaces of the sample.

The switching behavior of larger areas was also investigated. On the top electrodes of the samples, the entire region under the capacitor was poled and subsequently imaged in both polarization directions. Bare surfaces were also studied by poling large (2 μm) regions by scanning the region at a fast rate (2 Hz) with a tip held at a dc bias above the coercive voltage. Regions were poled with both positive and negative voltages, and were subsequently imaged. PFM images were obtained before and after the switching. +/-10 V_{dc} were used to pole the sample and the imaging voltage was 1 V_{rms}, a value below the coercive voltage of the sample.

2.3 Results

Measurements were performed both through the top electrodes and on bare surfaces for all three film thicknesses. We will first present results from the capacitors.

2.3.1 Top Electrodes

The results from imaging the top electrodes on the samples with thicknesses of 100, 300, and 500 nm are shown in figures 1, 2, and 3, respectively. The as-grown, positively poled, and negatively poled regions are shown. The topographic images have RMS surface roughnesses of 1.00, 0.78, and 0.76 nm for the 100, 300, and 500 nm thick samples, respectively. All of the images reflect an initial preference of the samples for the negative state (i.e. with the polarization vector pointing toward the bottom electrode). Some domains backswitched after poling in both directions. However, more domains backswitched from a positive state to a negative state than vice versa, shown by the histograms in figure 4.

Local measurements of d_{33} versus voltage were also performed. These loops revealed that some domains were shifted to the right, some to the left, and some were symmetric. The direction of the voltage shift corresponded to the backswitching behavior of the domain – domains that backswitched negatively were shifted to the right, domains that backswitched positively were shifted to the left, and those with no backswitching were symmetric. The shapes and offsets of the loops were repeatable, and representative loops taken from specific domains are shown in figure 5, 6, and 7.

2.3.2 Bare Surfaces

The topography and PFM images of the bare surfaces of the samples are shown in figures 8, 9, and 10. The topographic images have RMS surface of 0.81, 0.46, and 0.50 nm for the 100, 300, and 500 nm thick samples, respectively. Histogram analyses of the as-grown bare surfaces of all thicknesses reveal an initial preference for a negative polarization (Figure 11). As was the case when imaged through the top electrode, there was some backswitching from the positive polarization to the negative. However, no measurable backswitching occurred in the negatively poled regions.

As with the capacitors, d_{33} versus voltage measurements were obtained. These loops again revealed both positively and negatively imprinted domains, corresponding to the backswitching (i.e. domains backswitching from positive to negative were revealed to be negatively imprinted from the d_{33} versus voltage loops, while those not backswitching were symmetric or slightly positively imprinted). Representative loops from specific domains are shown in Figure 11.

The complete switching of the d_{33} loops demonstrates that the residual negative domains in the positively poled regions are not frozen (i.e. unswitchable), but have such strongly shifted hysteresis loops that they switch to the negative state even at zero volts, but otherwise switch normally to the positive state. Thus we can conclude that the negative domains are the result of backswitching.

2.4 Discussion

The samples have an initial preference for negative polarization and a tendency to backswitch from a positive polarization state to a negative one. While some

backswitching occurs from the negative state to positive in the measurements on capacitors, it occurs less often than backswitching from positive to negative. Furthermore, these backswitched domains exhibit a voltage shift in the opposite direction of the backswitching. This is strong evidence of a global negative imprint, as a shift in the voltage access of the hysteresis loop and backswitching are two of the main manifestations of imprint.

2.4.1 Imprint Mechanisms

Here we will discuss the bulk screening and interface screening models of imprint, both of which can explain the behavior of the samples investigated.

2.4.1.1 Bulk Screening

The bulk screening model posits that a thin interface layer exists between the electrode and ferroelectric layer [5, 6]. If there were no interface layer, charges at the electrode would completely screen the bound polarization charges, and no electric field would exist in the ferroelectric layer. With the interface layer, however, there is a spatial separation between the bound polarization charges and the mobile charges in the electrode. Thus a residual depolarizing field, E_{res}, arises in the ferroelectric layer [Figure 11].

The E_{res} is then compensated by electronic charges in the ferroelectric layer. The charges can then become trapped at the electrode/ferroelectric layer interface, screening the polarization. If the time constant of the charge redistribution exceeds the switching

time of the ferroelectric, the trapped charges can form an internal bias field that is the basis of imprint [7].

2.4.1.2 Interface Screening

The interface screening model is related to the bulk screening model. In the case of zero bias, in which the ferroelectric layer is polarized, but the top and bottom electrodes are shorted and no additional bias is applied, imprint is still observed [7]. The E_{res} must be compensated in order to satisfy the Maxwell equation

$$\oint \mathbf{E} d\mathbf{s} = 0 . \quad (1)$$

As a result, a field, E_{if}, forms in the interface layer, pointing in the direction of the polarization [Figure 12]. This field is the basis of interface screening. It can cause charge injection from the electrode or charge separation in the surface layer. Furthermore, at one of the electrode/ferroelectric layer interfaces, E_{res} and E_{if} will point toward each other, creating a condition conducive to charge trapping [7].

2.4.2 Influence of Capacitors on Imprint

Hysteresis loops from both the top electrode and the bare surface suggest that top electrodes moderate the negative imprint in the samples, and even introduce positive imprint in some regions. The negative imprint on the bare surface suggests the existence of trapped negative charges in the sample at the bottom electrode [Figure 12a] [8]. These charges are drawn to charged defects near the bottom electrode, thought to be oxygen vacancies [9]. This negative imprint occurs after the polarization is such that the negative bound charge is drawn to the electrode interface due to the two imprint mechanisms

described above. It is possible for the sample to become positively imprinted, but it is less likely, as positive space charge is less likely to become localized at the electrode interface.

Furthermore, the residual depolarizing field and interface layer field point toward at the bottom interface each other in the case of a negative domain with no top electrode. This creates an ideal trapping condition [7]. In the case of a top electrode, this trapping condition can occur at the bottom interface (for negative domains) or at the top interface (for positive domains). Thus imprint can occur in both directions, moderating the severe negative imprint detected without top electrodes.

The top electrodes introduce the same defects as the bottom electrodes and possess the same ability to trap negative space charge. Therefore positive domains can become imprinted by a negative space charge which becomes trapped by the positive bound polarization charges at the top electrode. Thus, it is possible for imprint to occur in either direction, depending on the polarization state [Figure 12b]. This explains 1) the moderation of imprint in the d_{33} loops and 2) the backswitching from negative to positive polarization states that occurs in capacitors, but not on the bare surface.

2.4.3 Influence of Film Thickness on Imprint

The thinnest film, 100 nm, exhibited the strongest imprint behavior of all samples both on the bare surface and under top electrodes, shown by the phase histograms. The 100 nm sample exhibits the same behavior as the other two – moderation of imprint upon electrode deposition. Therefore we assume that the imprint mechanism is the same.

In the thinnest sample the interface layer occupies a larger fraction of the capacitor than in the thicker ones. Thus, the interface dipoles exert a stronger force on the spontaneous dipole resulting from the polarization. This will have the effect of increasing the imprint in the sample. This thickness dependence of imprint correlates to the thickness dependence of the small-signal dielectric permittivity of Pt/PZT/Pt capacitors reported by Lee, *et al*. [10]. They did not observe a thickness dependence in PZT films with oxide electrodes, which was attributed to the electrodes act as a sink for oxygen vacancies.

2.4.4 Influence of Imprint on Hysteresis Loop

Regions exhibiting backswitching were shown to have d_{33} loops shifted along the voltage axis, consistent with prior results. Loops from these regions also exhibited narrower hysteresis loops than non-backswitching regions. This can also be attributed to trapped space charge in the imprinted regions creating competing imprint effects. The trapped space charge screens the bound polarization charge, reducing the magnitude of the polarization vector. The polarization vector then switches at lower voltages, resulting in a narrowed hysteresis loop.

2.5 Conclusions

In this study PFM was used to investigate the nanoscale mechanism of imprint in PZT thin films. It was found that negative domains tended to be more stable than positive domains, especially in measurements taken on the bare surface of the film, demonstrated by histogram analyses of regions after switching 1 μm^2 areas and by

voltage shifts of local d_{33}-V loops. This was attributed to an electric field generated by immobilized space-charge electrode interface which screened the bound polarization. The presence of capacitor structures lessened the severity of the imprint because they resulted in immobilized space charge at both electrode interfaces.

2.6 References

1. I. Inoue and Y. Hayashi, IEEE Transactions on Electron Devices, Vol. 48, No. 10, October 2001.
2. A. Gruverman, O. Auciello, and H. Tokumoto, Integr. Ferroelectr. **19**, 49 (1998).
3. G. Zavala, J. Fendler, and S. Trolier-McKinstry, J. Appl. Phys. **81**, 7480 (1997).
4. J. Christman, PhD thesis, North Carolina State University (1999).
5. V. Fridkin, *Photoferroelectrics, Solid State Sciences* (Springer, Berlin, 1979).
6. V. Shur and E. Rumyantsev, Ferroelectrics **191**, 319 (1997).
7. Grossman *et al*., J. Appl. Phys. **92**, 2680 (2002).
8. A. Gruverman, M. Tanaka, J. Appl. Phys. **89**, 1836 (2001).
9. I. Yoo and S. Desu, Phys. Status Solidi A **133**, 565 (1992).
10. J. Lee, C. Thio, and S. Desu, J. Appl. Phys. **78**, 5073 (1995).

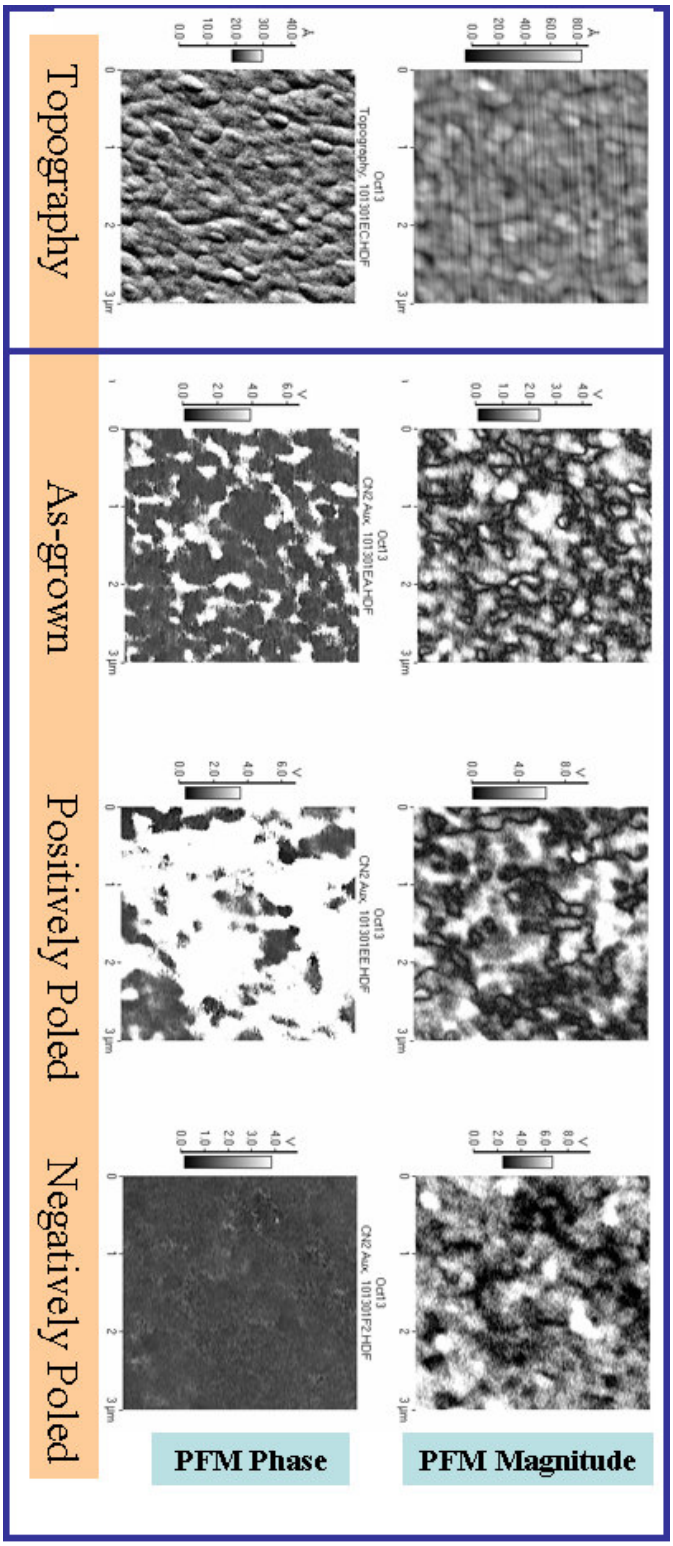

Figure 2.1 – Topography and PFM images of the 100 nm sample imaged through the top electrode.

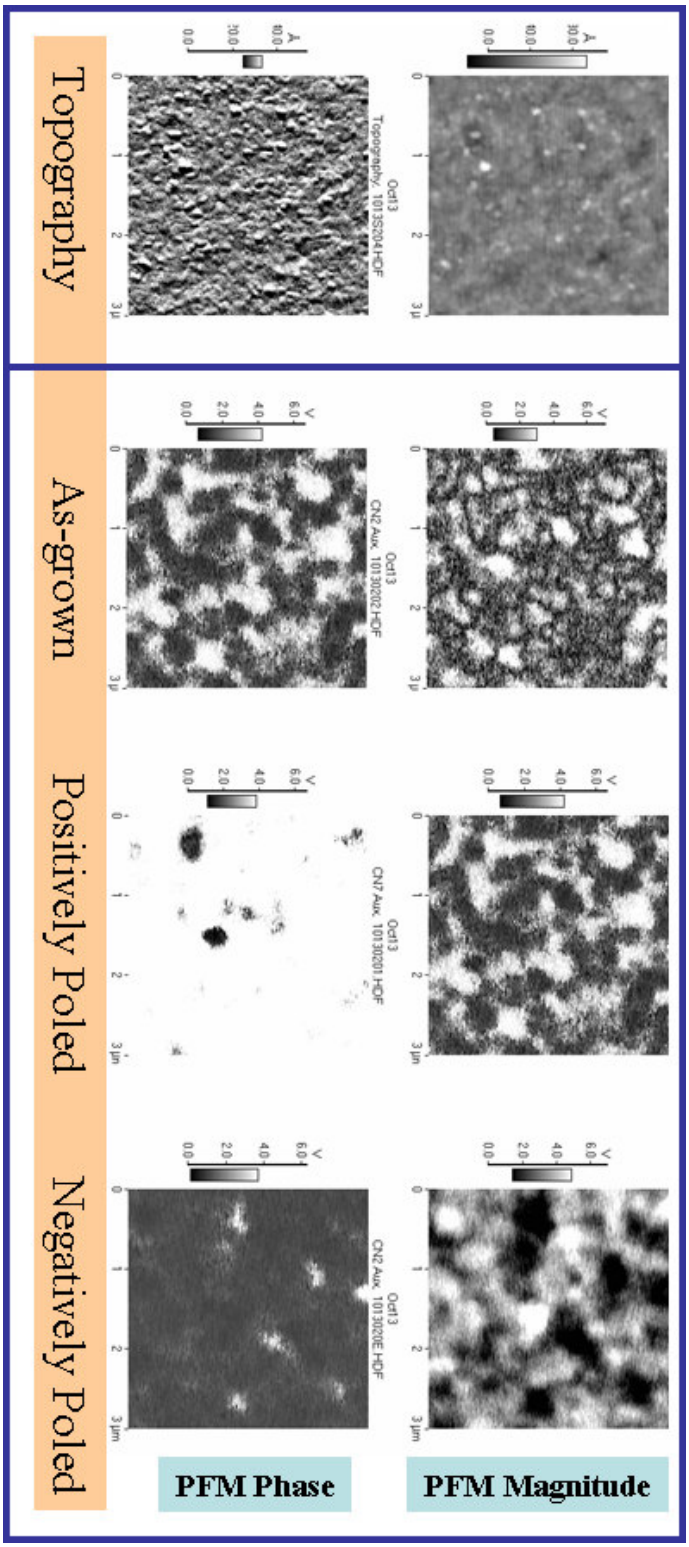

Figure 2.2 – Topography and PFM images of the 300 nm sample imaged through the top electrode.

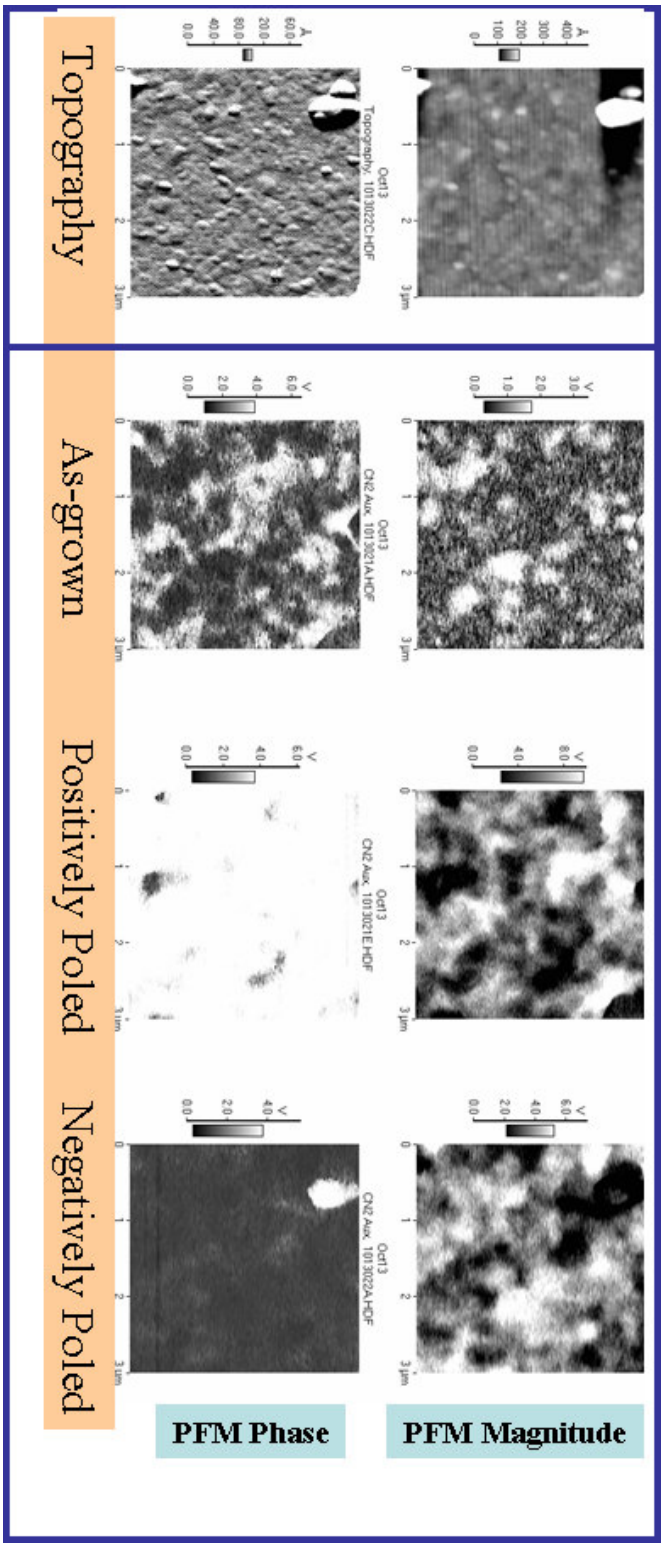

Figure 2.3 – Topography and PFM images of the 500 nm sample imaged through the top electrode.

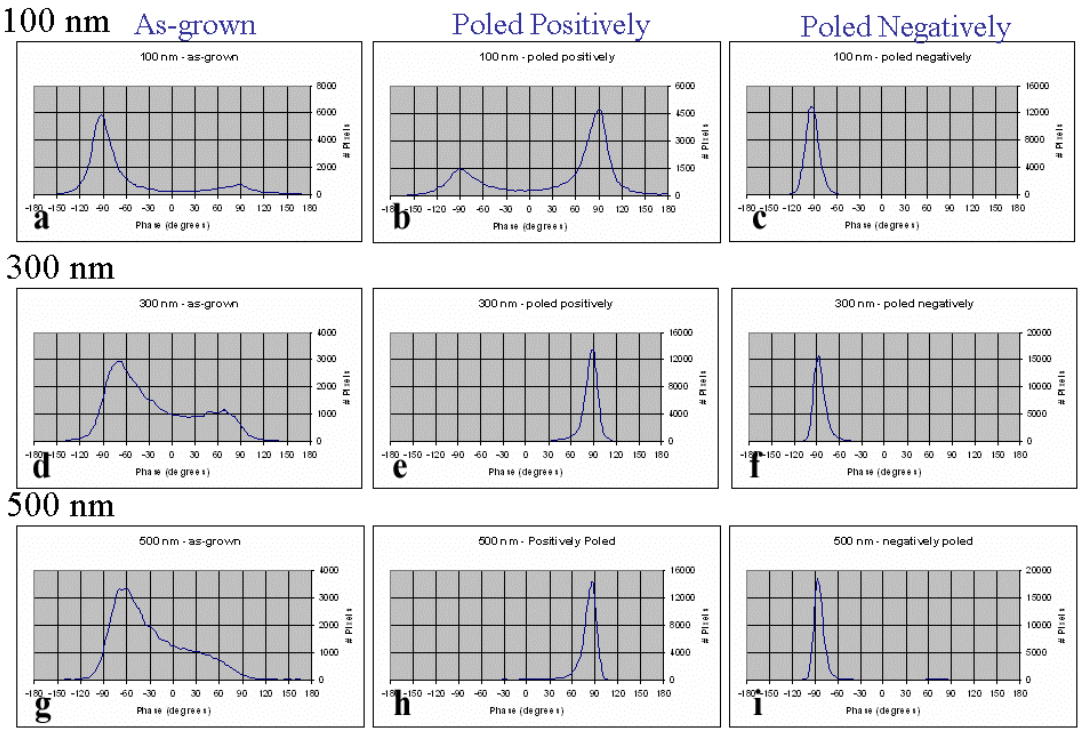

Figure 2.4 – Histograms of PFM phase images taken through the top electrode.

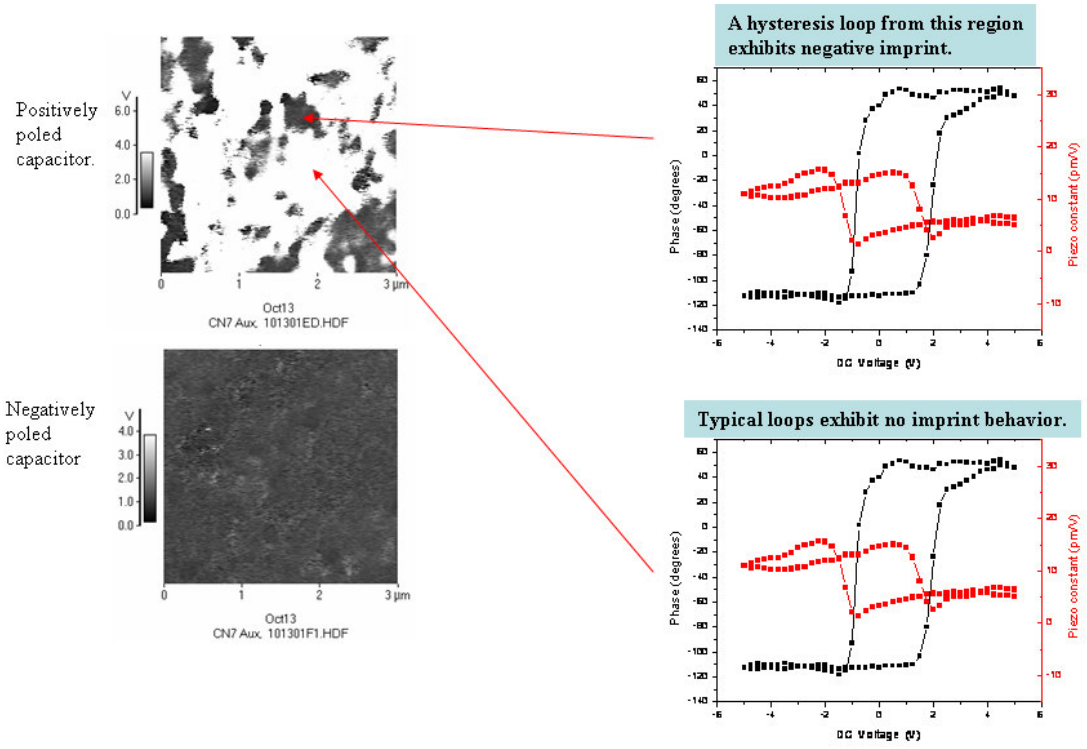

Figure 2.5 – Representative d_{33} – V from the 100 nm sample, imaged through the top electrode.

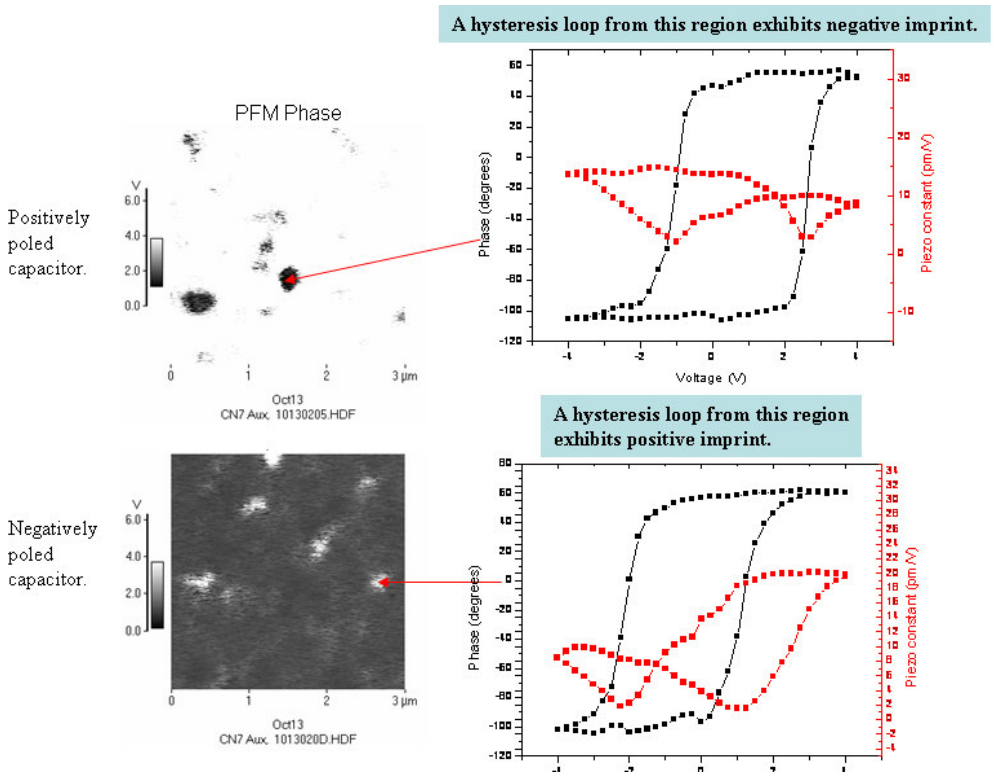

Figure 2.6 – Representative d_{33} – V from the 300 nm sample, imaged through the top electrode.

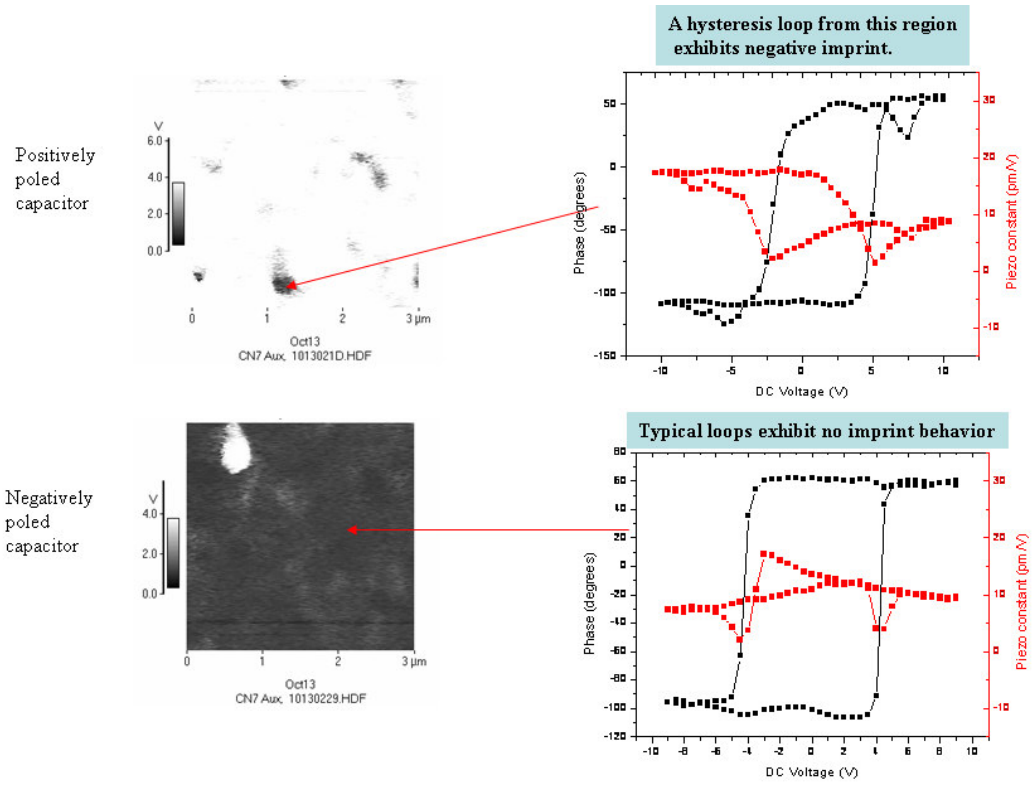

Figure 2.7 – Representative d_{33} – V loops from the 500 nm sample, imaged through the top electrode.

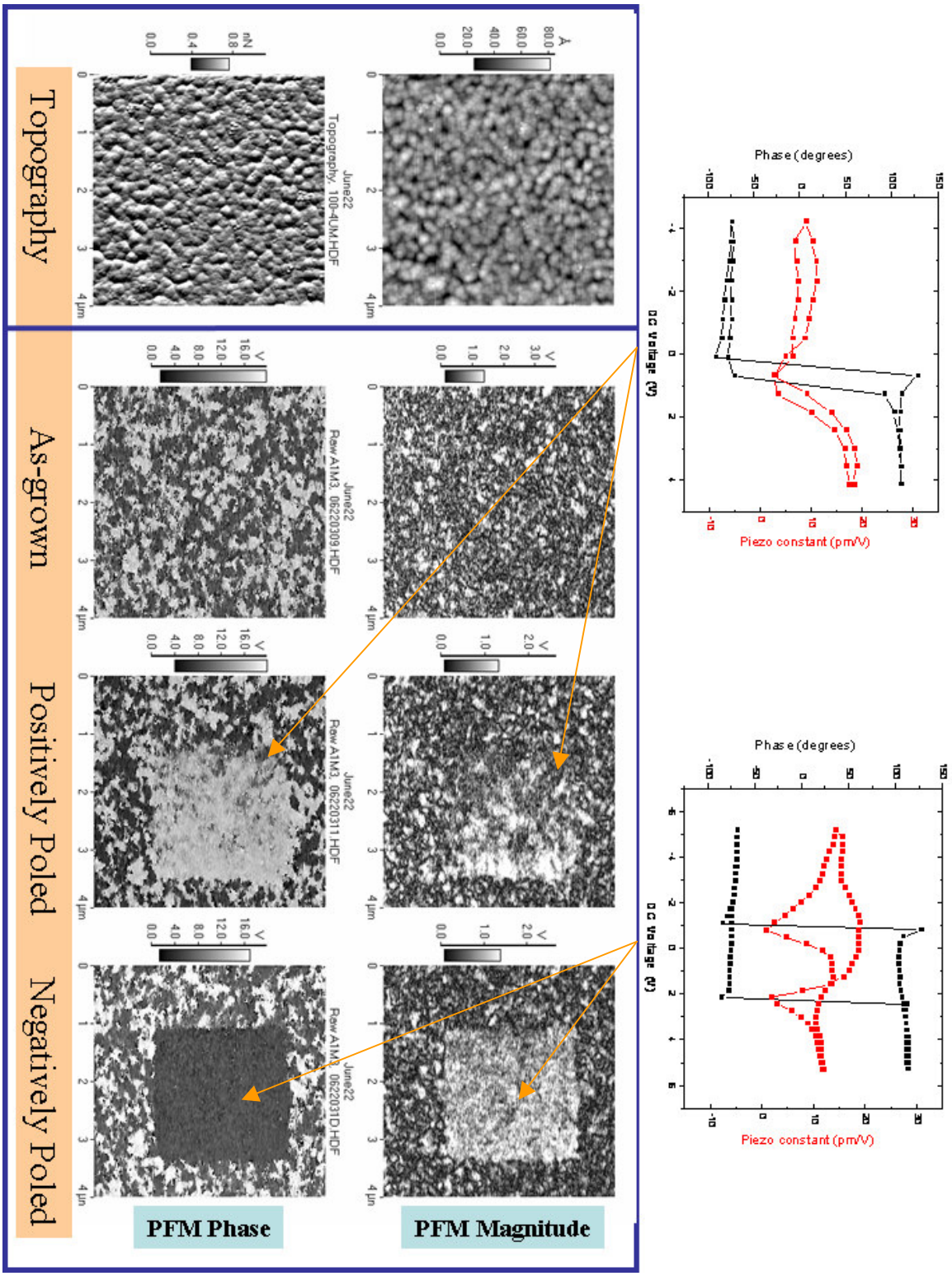

Figure 2.8 – Topography and PFM images of the 100 nm sample imaged on the bare surface, with representative d_{33}—V loops.

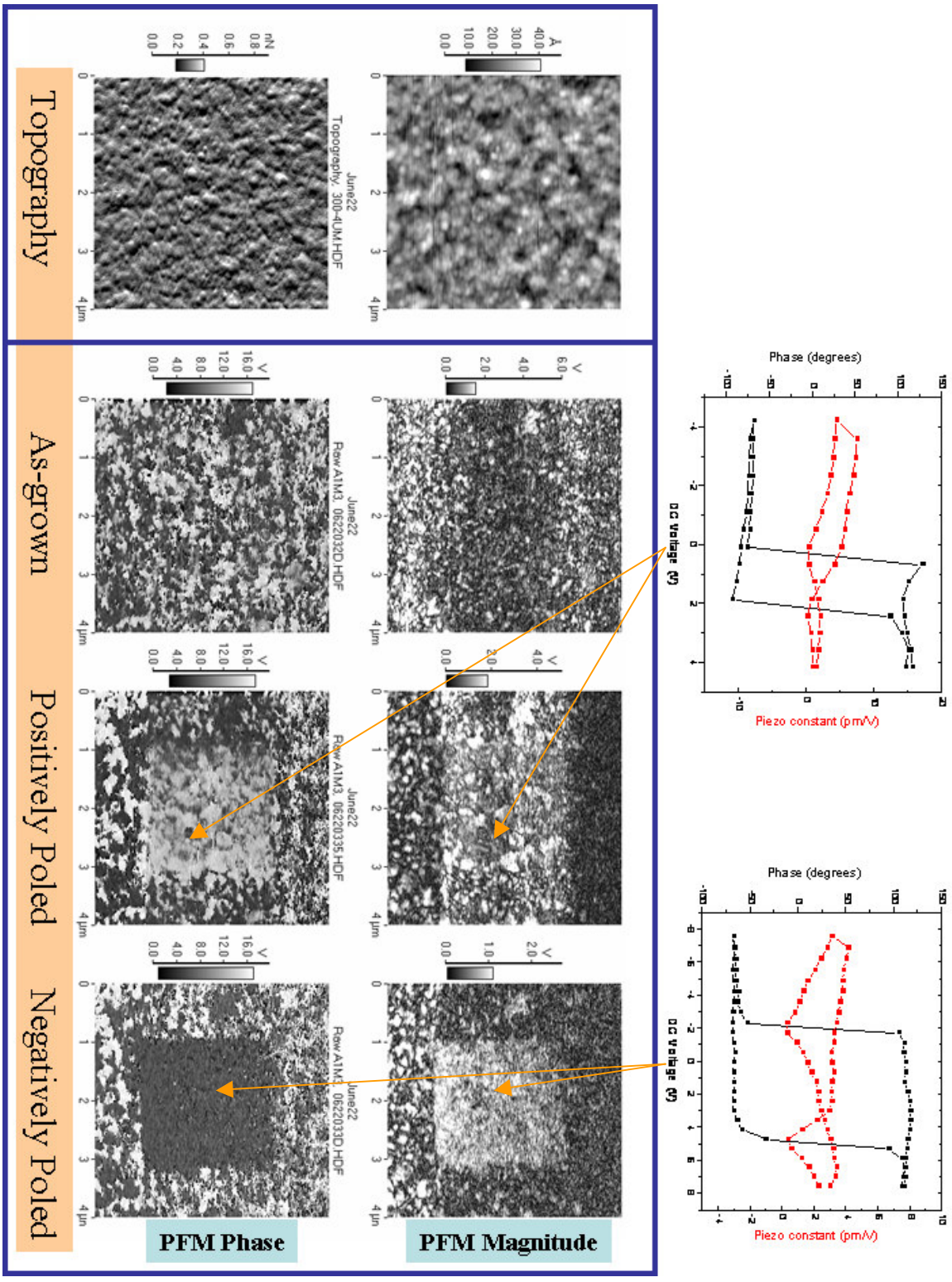

Figure 2.9 – Topography and PFM images of the 300 nm sample imaged on the bare surface, with representative d_{33}—V loops.

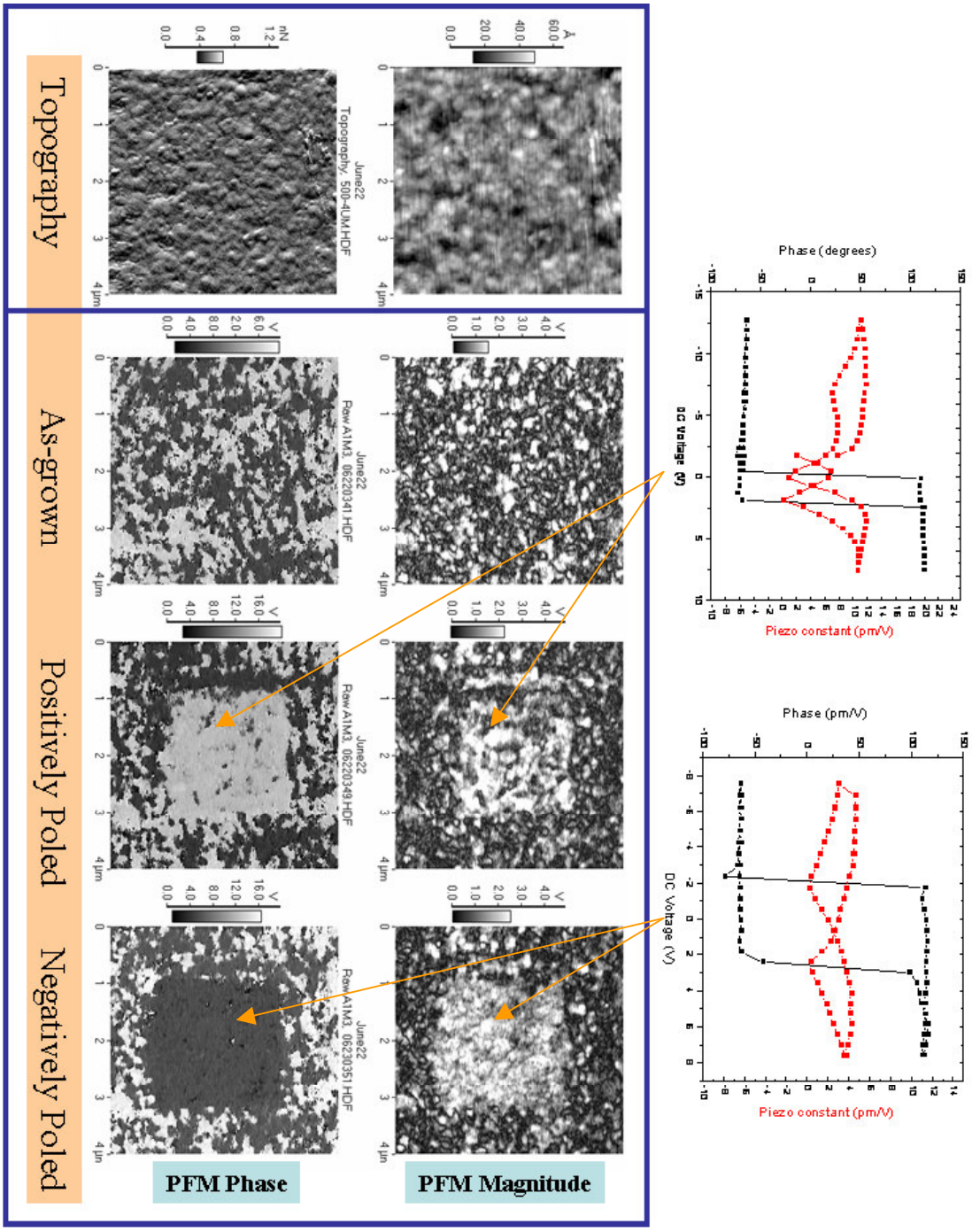

Figure 2.10 – Topography and PFM images of the 500 nm sample imaged on the bare surface, with representative d_{33}—V loops.

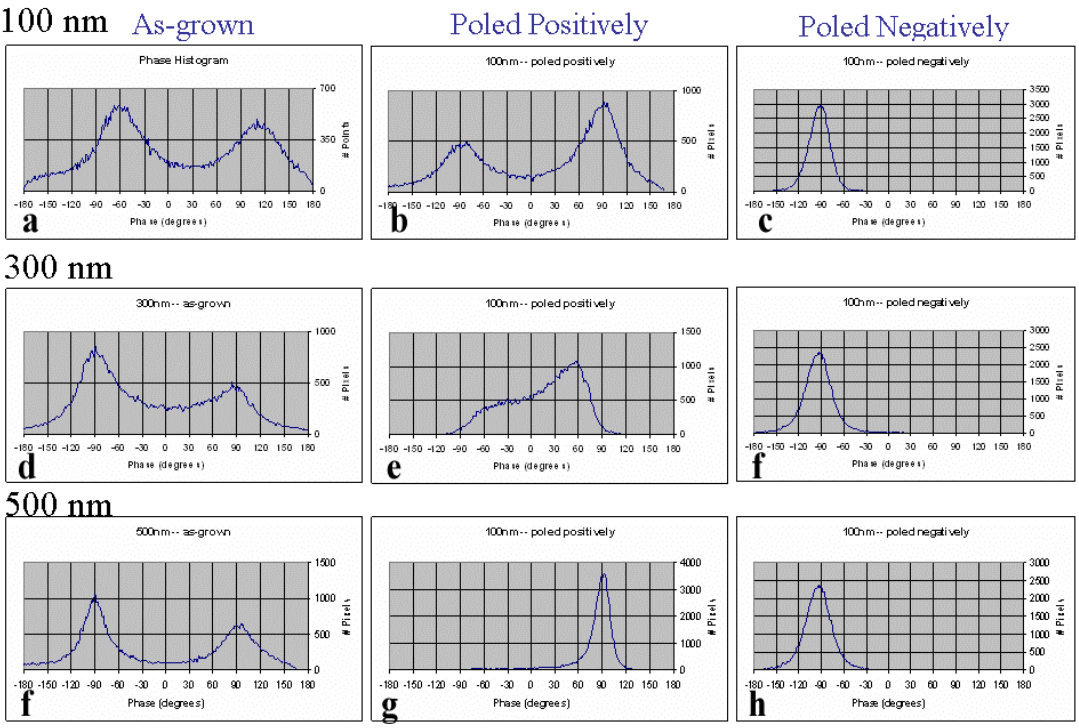

Figure 2.11 – Histograms of PFM phase images from bare surfaces.

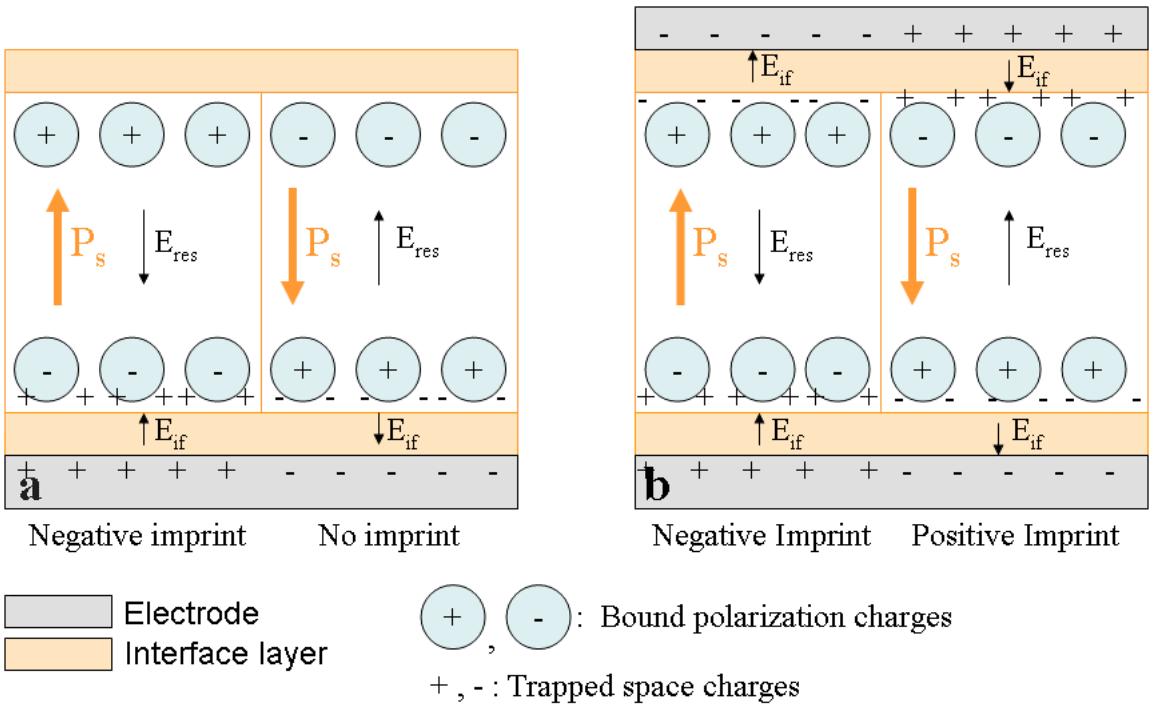

Figure 2.12 – Immobilized space charge (a) without top electrodes, and (b) with. In (b) imprint can occur in both directions, but only in one direction in (a). The residual depolarizing field (E_{res}) and interface field (E_{if}) are shown schematically.

Chapter 3: Fatigue Mechanisms in Ceramic PZT

3.1 Introduction

Fatigue, described in Chapter 1.5, is the loss of switchable polarization in ferroelectrics due to electrical stress [1]. It is a problematic degradation effect that can lead to failure in memory devices because it can render polarization values so low that they are difficult to resolve by sensors [2].

Piezoresponse force microscopy (PFM) can be used to directly image the domain structure of ferroelectrics, shedding light on the mechanisms by which fatigue occurs. In this study the domain structures of fatigued and virgin ceramic PZT samples were compared. The switching of the sample was then compared as a function of increasing voltage (at a very thin region), and as a function of sample thickness.

3.2 Experiment

Commercial disk-shaped PZT samples ($Pb_{0.99}[Zr_{0.45}Ti_{0.47}(Ni_{0.33}Sb_{0.67})_{0.08}]O_3$) (PIC 151, PI Ceramic Lederhose, Germany) were used for the experiment. The samples are on the tetragonal side of the morphotropic phase boundary; the Curie temperature is T_C = 250 ˚C, and the average grain size is ~6 μm. Silver electrodes were sputtered onto the sample, and the samples were cycled at 20 kV/cm, about twice the coercive field.

The samples were prepared by cutting the disk-shaped sample into two semi-circles. They were then embedded in epoxy resin, exposing the surface, and next polished at a 10˚ angle to a final finish of 0.25 μm. By polishing the sample in this manner it is possible to measure a wide range of thicknesses, from 0 to about 700 μm.

The fatigued samples had a final positively oriented polarization vector as a result of the poling. The orientation of the polarization vectors in the virgin sample was random.

Measurements were performed using PFM [3,4]. A more detailed description of PFM is given in Chapter 1.4. To summarize, an ac voltage is applied to a conducting AFM tip in contact with the surface. The resulting mechanical oscillation of the surface due to the converse piezoelectric effect can be detected using a standard lock-in technique. The amplitude of the oscillation is proportional to the longitudinal piezoelectric coefficient, and the phase of the oscillation describes the orientation of the out-of-plane polarization vector. A stiff (k = 50 N/m) cantilever was used. The imaging voltage depended on the sample thickness, and was applied at 12 kHz.

The switching behavior of 10×10 μm^2 areas was investigated. The surfaces were studied by poling regions by scanning the region at a fast rate (2 Hz) with a tip held at a dc bias. 20×20 μm^2 regions were poled positively to obtain a uniform polarization direction. Next, 10×10 μm^2 regions was poled negatively and subsequently imaged in discrete voltage steps in order to determine the percentage of the area switched as a function of voltage.

3.3 Results

3.3.1 Domain Structure

PFM images were obtained at the same thickness for both fatigued (cycled 1.7×10^7 times) and virgin (cycled zero times) samples. Domain and grain boundaries

were identified both by eye [Figure 1] and with the image processing program SPIP (Image Metrology, Denmark) [Figure 2]. The average number of regions per square micron was higher in the fatigued samples than in the virgin ones. Four sets of images were analyzed – two from the virgin sample and two from the fatigued. According to the image processing program, 0.089 domains plus grains per square micron were detected for the virgin sample, as opposed to 0.15 for the fatigued sample. By eye, 0.075 domains plus grains per square micron were detected for the virgin sample, as opposed to 0.15 for the fatigued.

3.3.2 Fatigue Effects on Area Switching

All samples were poled positively prior to PFM measurements, so a homogeneous positive polarization was expected. However, residual domains were observed, the number and size increasing with the fatigue state [Figure 3]. The residual domains were not "frozen" and could be poled in either direction.

A 20×20 μm^2 region was poled positively to remove residual domains, and a 10 μm^2 region was then poled negatively with increasing voltages. An example of the procedure is shown in Figure 4. The completeness of the switching was measured by analyzing the number of black and white pixels in the image. Graphs of percentage of image switched versus applied dc voltage for virgin, fatigued (3×10^7 cycles), and semi-fatigued (3×10^5 cycles) are shown in Figure 5 a). There are only small differences between the switching curves, and they are not deemed to be statistically significant.

The macroscopically obtained fatigue profiles are shown in Figure 5 b).

3.3.3 Compositional Effects on Area Switching

Compositional effects on switching were also observed. Three samples were fatigued for 3×10^7 cycles. One sample had silver electrodes, and two had platinum electrodes, but were from different sinter batches. The macroscopic fatigue curves from the fatigued samples are shown in Figure 6. The results of the microscopic area switching experiments for both sets of samples (virgin and fatigued for 3×10^7 cycles) are shown in Figure 7.

3.3.4 Backswitching

No backswitching was observed near the interfaces. However, in thicker parts of the sample, complete backswitching occurred. Figure 8 shows images taken from a sample with silver electrodes fatigued 3×10^7 cycles with a thickness of 450 μm. When the ac imaging voltage was summed with 50 V dc, complete switching was observed. However, immediately following this simultaneous poling and imaging scan, an imaging scan with no dc bias was taken, revealing nearly complete backswitching. Backswitching shows a strong thickness dependence in the fatigued sample but is absent in the virgin sample.

3.4 Discussion

3.4.1 Domain Structure

The fatigued samples have a significantly higher domain density than the virgin samples, reflecting the formation of new domain walls. Others have observed a correlation between domain density and fatigue, but also observed "wavy" domain walls attributed to ferroelastic twinning [5]. Here we did not see wavy domains, but did observe an increase in the ratio of domain perimeter to domain area, suggesting that the domains tend to become more complex. This can be attributed to the clustering of point defects observed in bipolar fatigue [6,7]. These point defects can induce preferred polarization states in regions immediately surrounding them, restricting growth in one direction while encouraging it in the other.

Thus, as the sample cycles between polarization states, more and more defects cluster, inhibiting switching at specific points and leading to an increasingly complex domain structure.

3.4.2 Fatigue Effects on Area Switching

Figure 5 demonstrates no significant difference between the amount of fatigue in a sample and the switching – voltage curves. There are several possible reasons why this experiment failed to yield any differences between the differently fatigued samples:

1) The field enhancement of a sharp tip provokes switching even in regions in which switching is normally restricted [8].
2) The uncertainty of the method is so great that it masks the true switching trend of the samples.

3) The sample preparation (embedding in epoxy and polishing) "refreshes" the sample through the mechanical stress that it is subjected to.

We believe that the first two possibilities are the most likely, as other samples and other techniques (such as domain structure imaging, backswitching measurements, and area switching in similar sample sets) have yielded significant differences.

3.4.3 Compositional Effects on Area Switching

The microscopic results from the area switching experiments correlate as expected with the macroscopic fatigue profiles. Samples completely switching only at high voltages demonstrate higher levels of fatigue than those that switching at low voltages.

The effect of electrode composition on fatigue behavior is well-known [1]. It is believed the electrode composition affects the number and nature of defects in the ferroelectric layer, explaining, for example, the superior fatigue behavior in samples with oxide electrodes [9,10,11]. These results demonstrate that silver electrodes have superior fatigue behavior compared to platinum, but also that the differences between sinter batches can be dramatic. It is unknown what processing steps were varied in these commercial samples.

3.4.4 Cascaded Backswitching Model

Figure 9 shows a strong thickness dependence of the backswitching of the fatigued sample, and no backswitching at any thickness in the case of the virgin sample. This can be explained by the cascaded switching model of fatigue [12].

Switching occurs across grain boundaries in part because a polarization mismatch occurring at the grain boundaries induces switching in adjacent grains. Grain boundaries are natural locations for the clustering of defects that hinder switching. As a sample is cycled charged defects cluster around such features [6], leading to charged grain boundaries that provide a preferred domain direction. In the absence of the applied poling field, the charged domain boundary provokes switching, which by the cascaded switching effects leads to backswitching up to the surface [Figure 10].

This model depends on negative doping of the sample, as is caused by oxygen vacancies, the most mobile ionic defects of perovskites [1]. Negative charges tend to "pull" the polarization vector toward them. Thus above a negatively charged grain boundary, the polarization vectors will tend to be negative, and cascaded backswitching will in turn induce backswitching in the grains above them. This hypothesis can be tested by measuring backswitching as a function of doping.

The influence of fatigue on backswitching is then explained by the absence of charges congregating at the grain boundaries due to voltage cycling.

The influence of thickness on backswitching can be explained by the greater number of grain boundaries underneath the thick part of the sample. As more charged grain boundaries exist, the probability that one will provoke cascaded backswitching increases.

3.5 Conclusions

1) The domain structure of the samples, as imaged by PFM becomes more complex. We suggest that this is caused by the accumulation of charged defects which hinder switching and force domains to grow around them.

2) Experiments were performed in which $10\times10\ \mu m^2$ areas of samples in three different fatigue states were poled by a scanning tip held at successively increasing dc voltages. Analysis of the amount of area switched as a function of the poling voltage yielded no significant differences between the samples, although macroscopic results from P(E) measurements revealed significant differences. It is believed that the error present in these experiments is greater than the differences between the samples, rendering the results inconclusive.

3) Similar area switching experiments were performed to measure the effects of electrode material and ferroelectric layer composition on fatigue. Significant differences were found between silver and platinum electrodes, with the silver electroded material exhibiting superior fatigue behavior. Two samples from different sinter batches, both with platinum electrodes, were discovered to have significant differences for unknown reasons.

4) Samples were scanned with ac and dc biases applied simultaneously. They were then scanned with an ac bias alone to determine if backswitching occurred in the absence of the dc voltage. The fatigued sample was revealed to have significant backswitching

that increased with thickness, while the virgin sample exhibited very little backswitching at any thickness. This behavior was explained by 1) charged grain boundaries introducing a preferred polarization direction in grains, and 2) cascaded switching [12], which holds that a grain with one polarization state induces nearby grains to switch in the same direction.

3.6 References

1. A. Tagantsev, I. Stolichnov, E. Colla, and N. Setter, J. Appl. Phy. **90,** 1387 (2001).
2. R. Waser, *Nanoelectronics and Information Technology* (WILEY-VCH GmbH & Co. KGaA, 2003.
3. A. Gruverman, O. Auciello, and H. Tokumoto, Integr. Ferroelectr. **19**, 49 (1998).
4. E. Colla, D. Taylor, A. Tagantsev, and N. Setter, Appl. Phys. Lett. **72**, 2763 (1998).
5. Q. Tan, Z. Xu, J. Li, and D. Viehland, J. Appl. Phys. **80**, 5866 (1996).
6. J. Nuffer, D. Lupascu, and J. Rödel, Acta Mater. **48**, 3783 (2000).
7. D. Lupascu and U. Rabe, Phys. Rev. Lett. **89**, 1876011 (2002).
8. S. Kalinin, A. Gruverman, B. Rodriguez, J. Shin, A. Baddorf, E. Karapetian, M. Kachanov, J. Appl. Phys. **97** 074305 (2005).
9. S. Bernstein, T. Wong, Y. Kisler, and R. Tustison, J. Mater. Res. **8**, 12 (1993).
10. O. Auciello, K. Gifford, D. Lichtenwalner, R. Dat, H. Al-Shareef, K. Bellur, and A. Kingon, J. Appl. Phys. **77**, 2146 (1994).
11. J. Cross, M. Fujiki, M. Tsukada, Y. Kotaka, and Y. Goto, Integr. Ferroelectr. **21**, 263 (1998).
12. G. Arlt and J. Calderwood, Appl. Phys. Lett. **81** 2605 (2001).

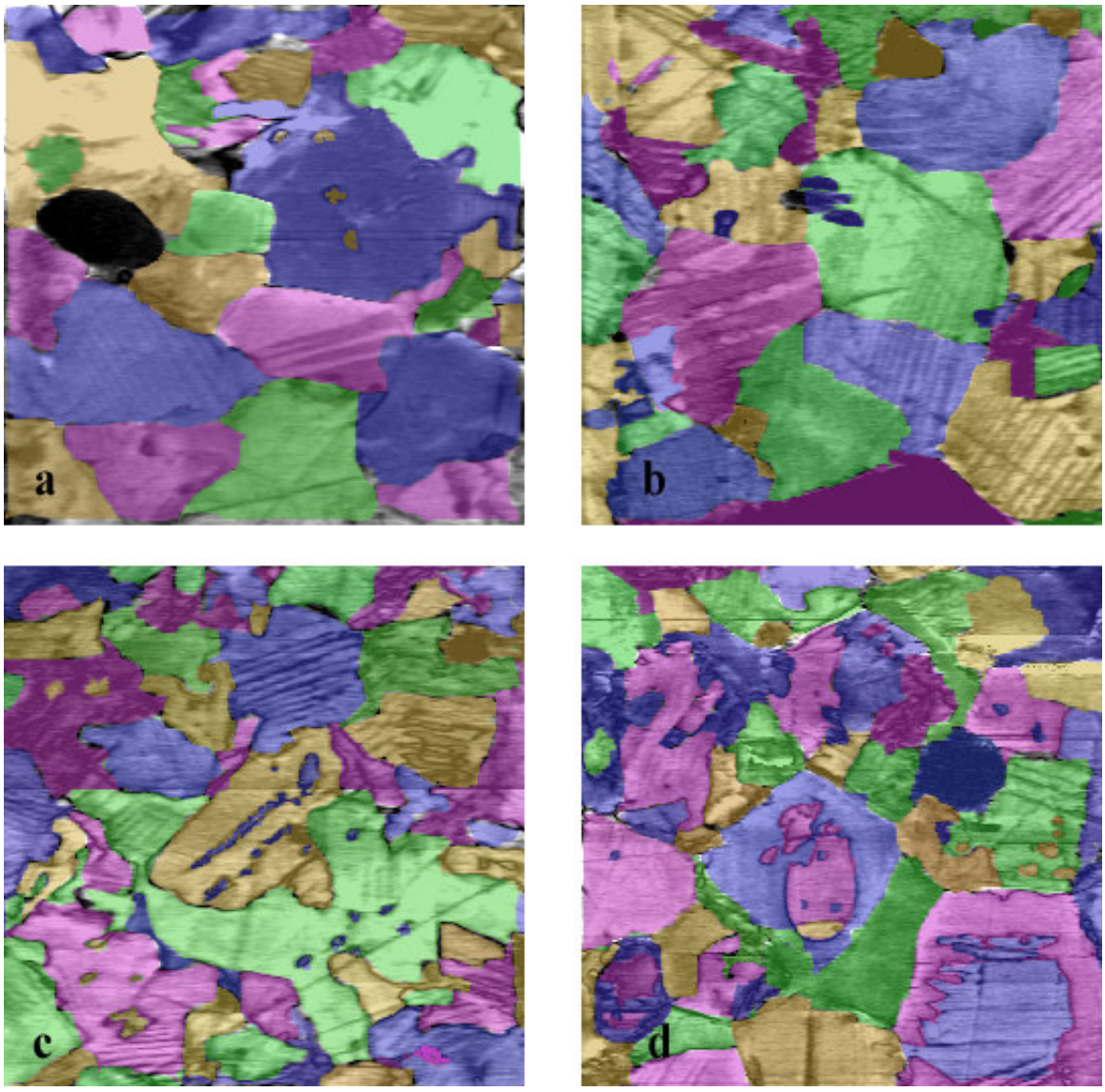

Figure 3.1 – Domain analysis of PFM amplitude image, with domains distinguished by eye.

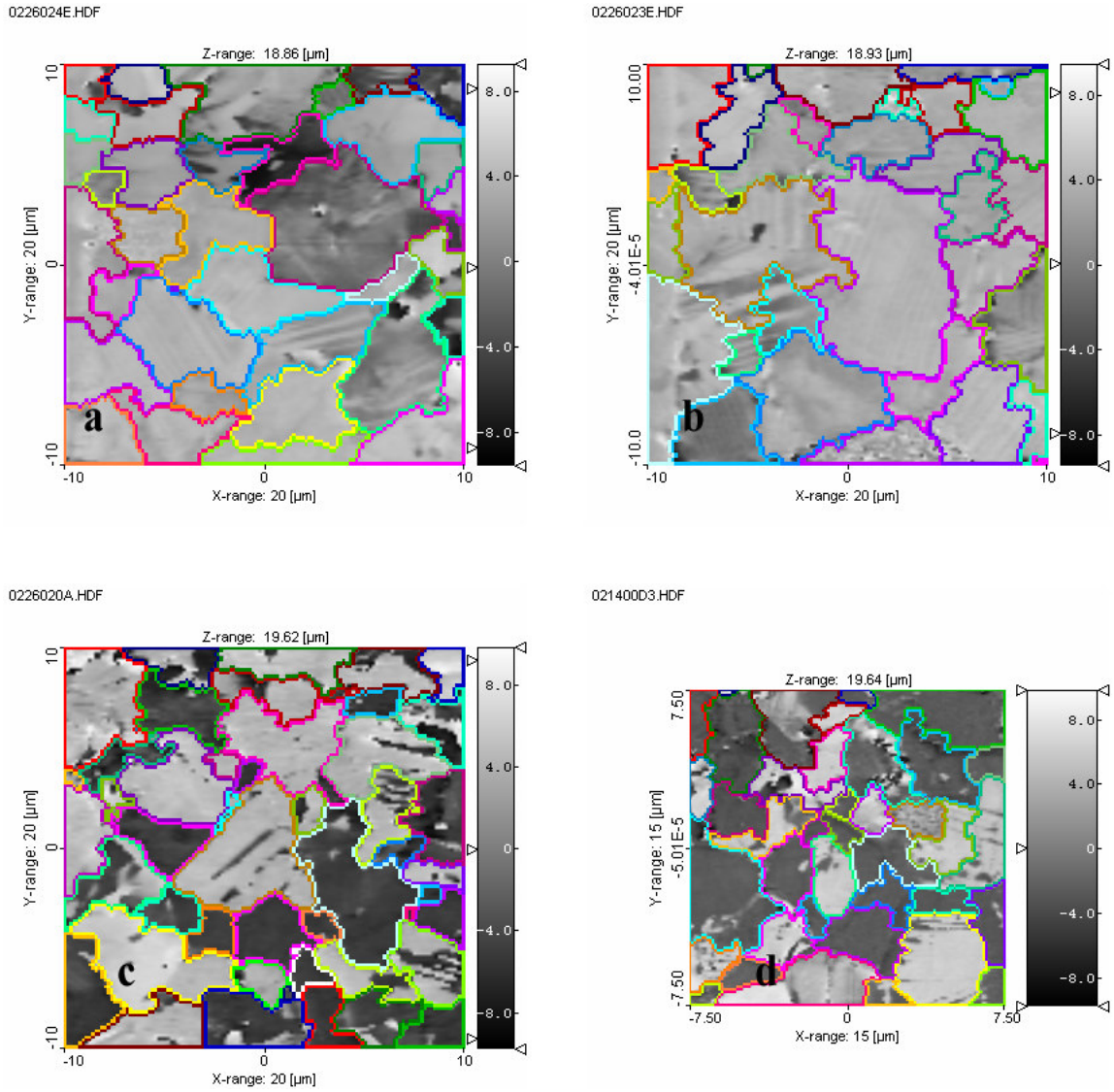

Figure 3.2 – Domain analysis of PFM amplitude image, with domains distinguished by the image processing program SPIP.

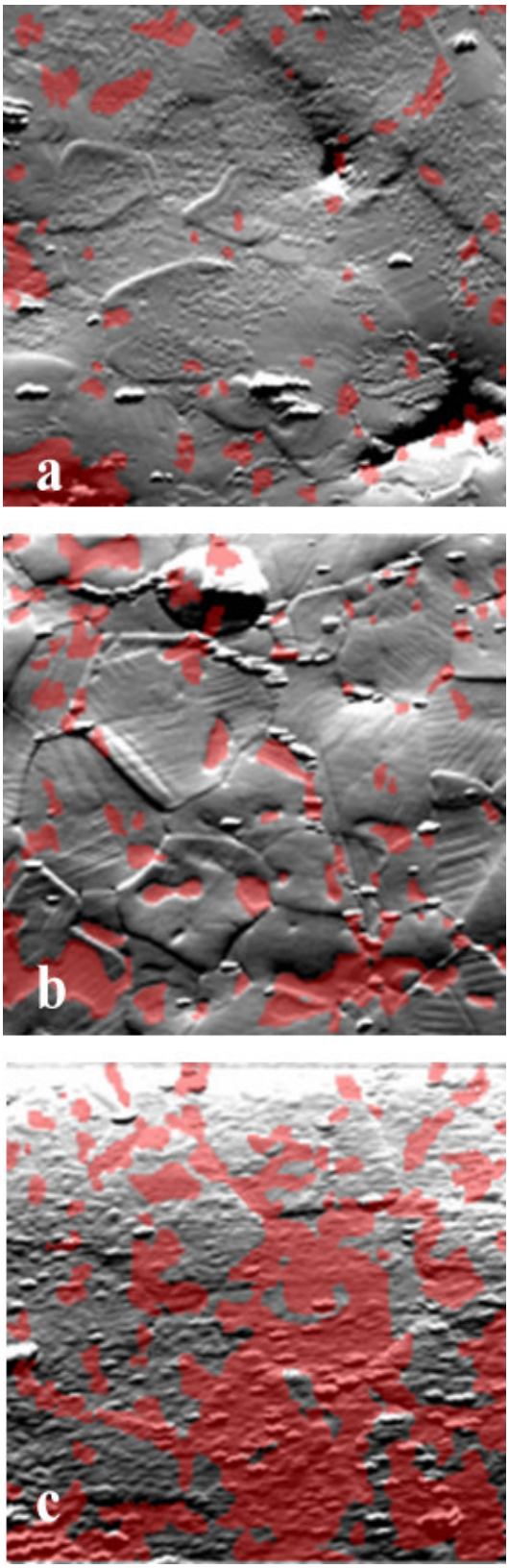

Figure 3.3 – Residual domains as a function of fatigue. The images were cycled a) 0, b) 3×10^{5}, and c) 3×10^{7} times.

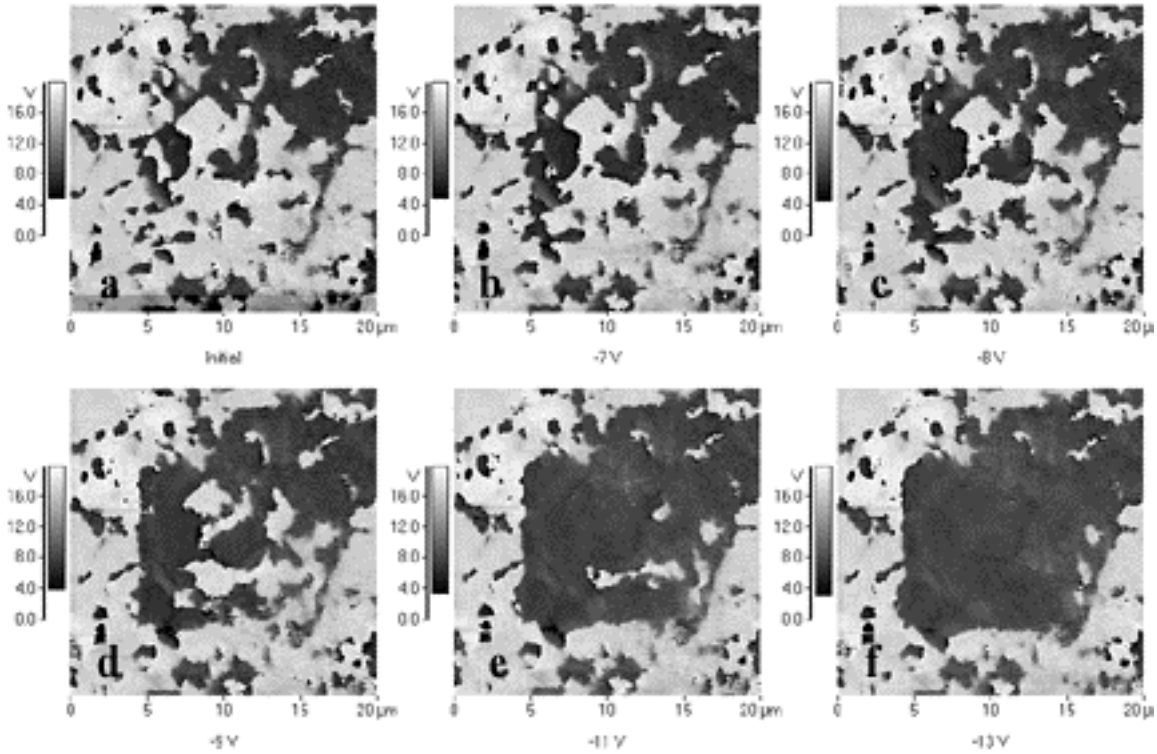

Figure 3.4 – An example of step-by-step area switching. The PFM phase images shown were taken after applying a) 0 V, b) -7 V, c) -8 V, d) -9 V, e) -11 V, and f) -13 V poling scan to a 10×10 μm^2 region in the center.

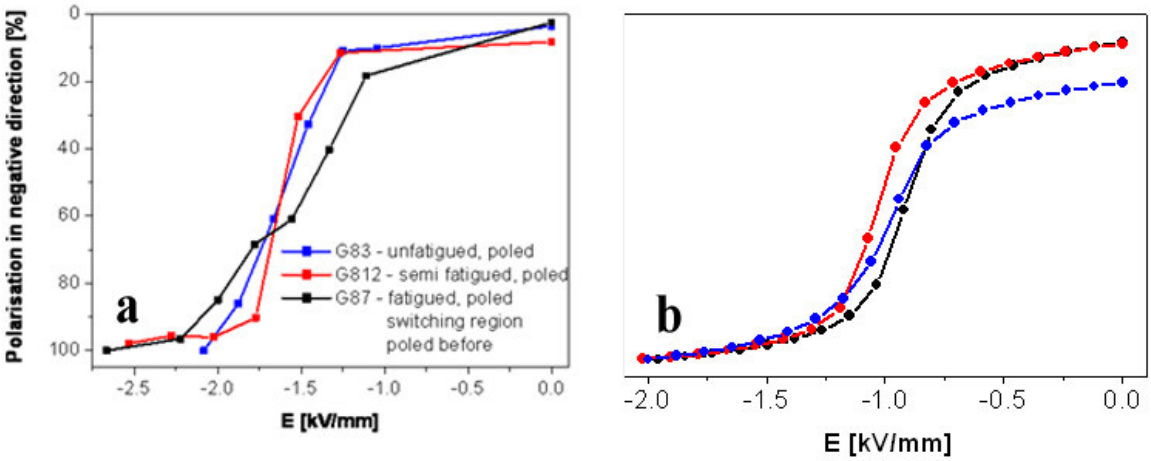

Figure 3.5 –Percent of sample in negative state versus applied field from a) microscopic area switching experiments, and b) macroscopic P(E) curve.

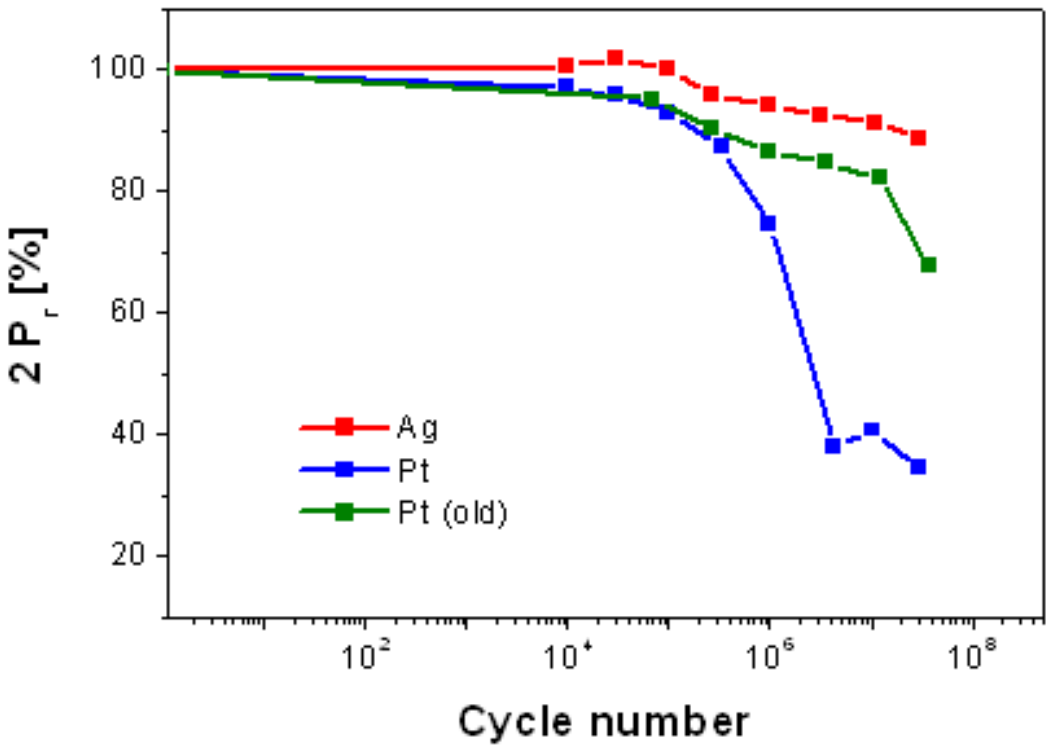

Figure 3.6 – Fatigue curves for silver electrodes, platinum electrodes on the second sinter batch, and platinum electrodes on the old sinter batch.

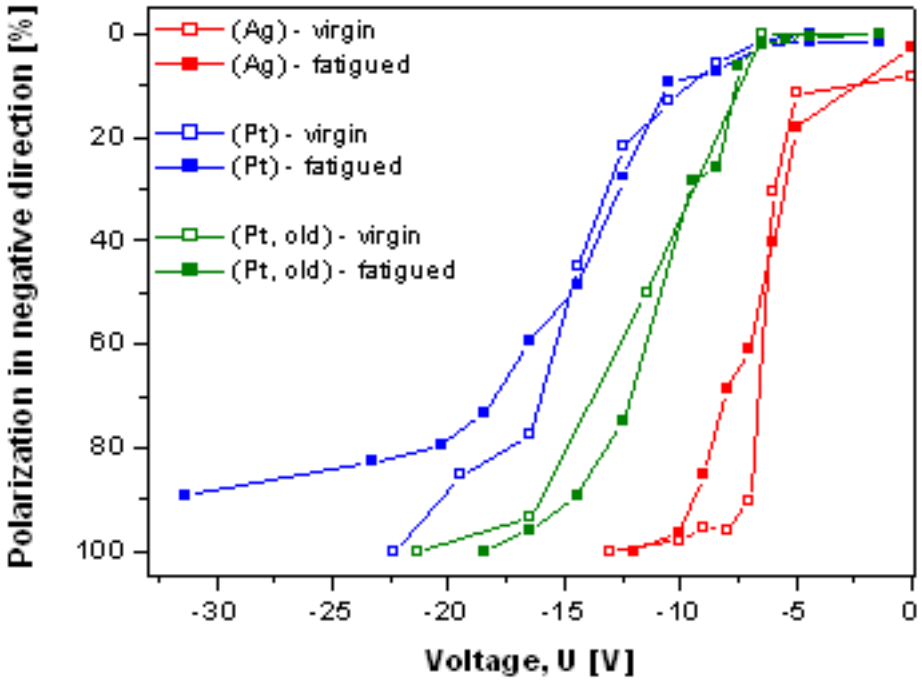

Figure 3.7 – Percent of negative domains from microscopic area switching experiments for silver electrodes, platinum electrodes on the new sinter batch, and platinum electrodes on the old sinter batch.

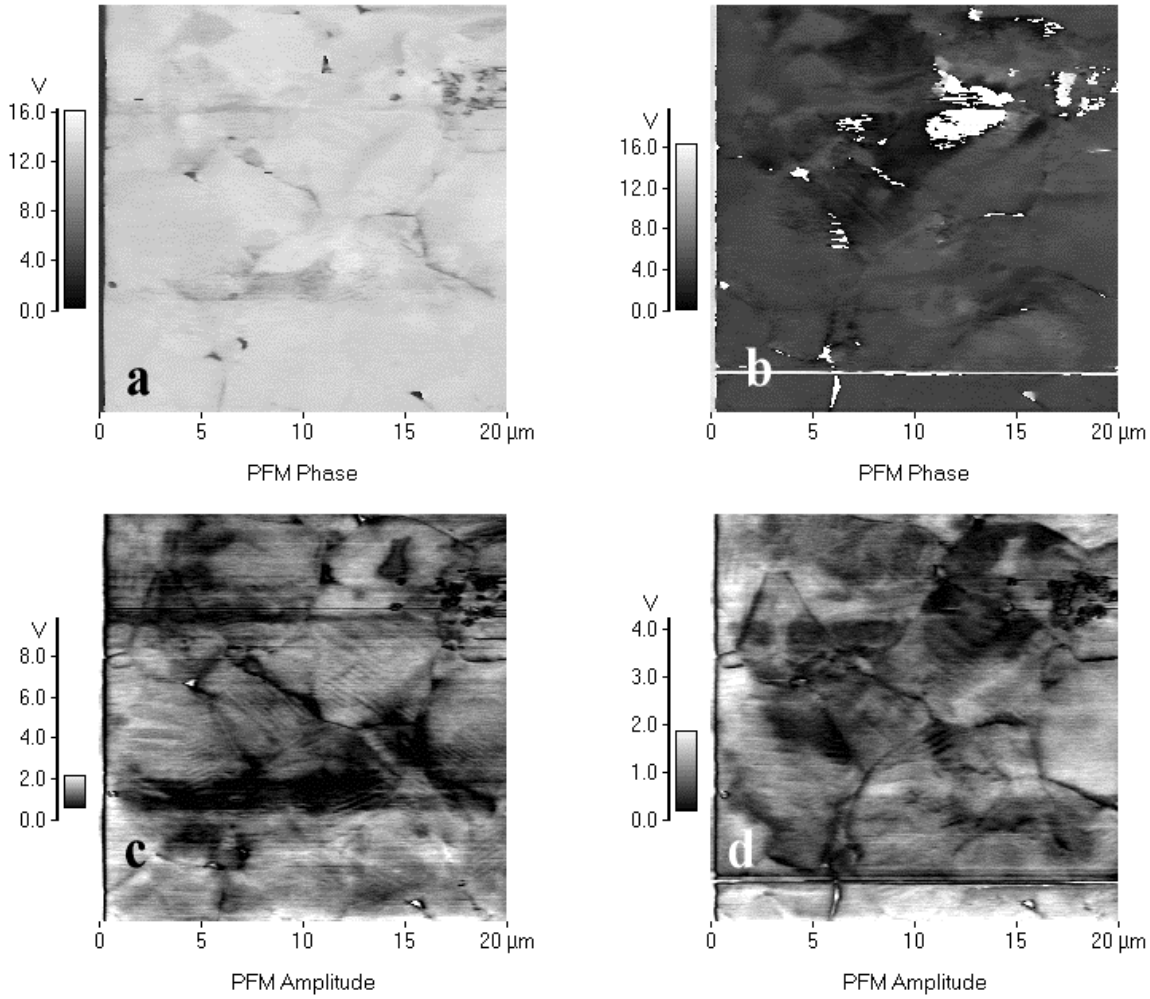

Figure 3.8 – PFM images demonstrating backswitching; a) and c) are the phase and amplitude images taken with a scan where +50 V_{dc} was applied in addition to the driving voltage. b) and d) were taken immediately afterward, and is almost completely switched negatively.

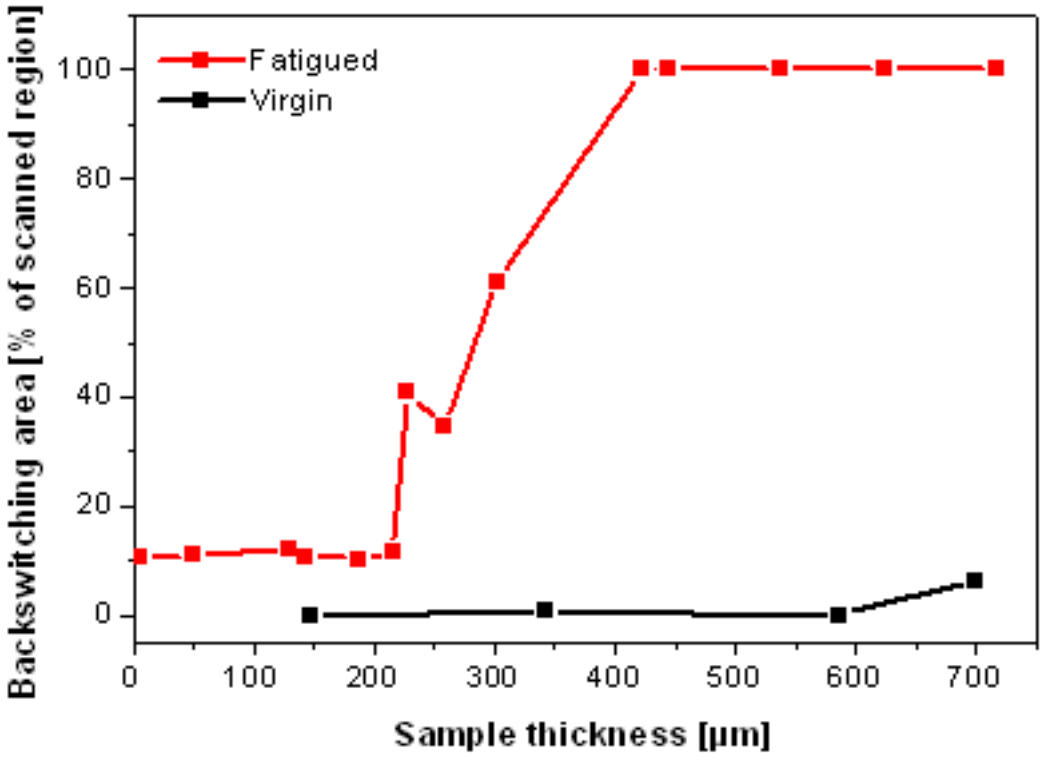

Figure 3.9 – Percent of area backswitched vs. sample thickness taken on virgin and fatigued samples with silver electrodes.

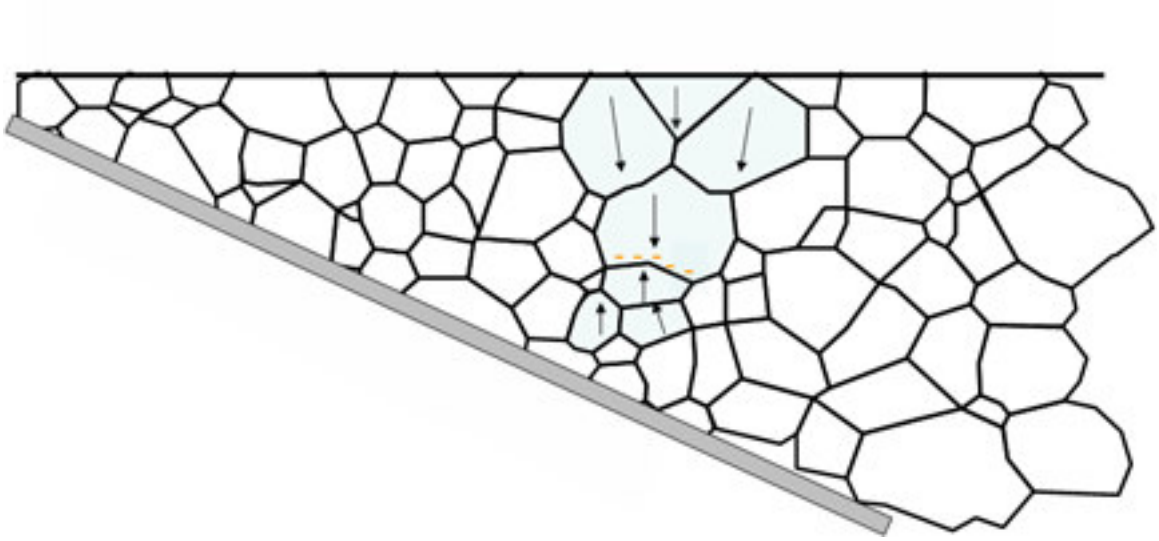

Figure 3.10 – Cascaded backswitching provoked by negative charges agglomerating at a grain boundary.

4. Summary and Future Work

4.1 Summary

The nanoscale manifestations of two ferroelectric degradation effects (imprint and fatigue) in lead zirconate titanate (PZT) thin films and ceramics were investigated using piezoresponse force microscopy (PFM). PFM is a variant of atomic force microscopy (AFM) by which a conducting tip measures piezoelectric behavior via the converse piezoelectric effect. Images were obtained for micron-scale regions. Spectroscopic measurements of d_{33}-V loops were obtained in regions whose size is governed only by the tip radius, 20-30 μm.

Imprint is the preference of a ferroelectric material for one polarization state over another. It manifests itself by a shift of the hysteresis loop along the voltage axis and by spontaneous backswitching in the absence of an electric field. Imprint was studied by investigating three PZT thin films with thicknesses of 100, 300, and 500 nm. The samples had regions with top electrodes as well as regions with only the bare surface exposed. Imprinted manifested itself by shifts in the locally obtained d_{33}-V loops and by spontaneous backswitching. The presence of top electrodes moderated the imprint in the samples. This effect was explained by the symmetry conditions of trapped charge caused by the electrodes. In the case where there is no top electrode, charge trapping occurs only along the bottom electrode interface, resulting in imprint in only one direction. In the case where there are also top electrodes, charge trapping occurs at both interfaces, moderating the amount of imprint.

Fatigue is the loss of polarization due to repeated switching. It was studied by investigating PZT ceramics in one of three fatigue states: virgin (cycled zero times),

semifatigued (cycled 3×10^5 times), and fatigued (cycled 3×10^7 times). The samples were polished at a wedge so that fatigue could be studied as a function of thickness. It was found that fatiguing a sample provoked changes in the domain structure, creating smaller, more complex domains. This was attributed to charged defects preventing domains from growing symmetrically. It was also found that severe backswitching occurred in the thick (>500 μm) regions of the sample. This effect was explained by the cascaded backswitching model, which posits that charged defects agglomerate at grain boundaries in the bulk, caused by the repeated switching. These charged defects then create a preferential polarization direction in certain grains. The polarization mismatch then provokes switching in the grain above it, and so on, until backswitching occurs at the surface. This model accounts for the existence of backswitching and its thickness dependence, as thick regions are more likely to contain charged defects at grain boundaries.

4.2 Future Work

4.2.1 Imprint

The results presented in Chapter 2 demonstrated the dependence of imprint on thickness and the presence of top electrodes. While the 100 nm samples was shown to be more severely imprinted than the 300 or 500 nm samples, the difference in imprint behavior between the latter two samples was small. With samples in the thickness range between 100 and 300 nm, as well as films below 100 nm, it may be possible to obtain a more detailed trend of imprint behavior as a function of thickness. For example, it is

possible that there are critical thicknesses at which point the imprint behavior changes drastically.

Secondly, the effects of electrode composition could be explored. It is commonly believed that imprint is caused at least in part by oxygen vacancies. The effects of oxide electrodes, which act as sinks for oxygen vacancies, could be explored, again as a function of film thickness. Other electrode metals such as silver and copper could be similarly explored.

4.2.2 Fatigue

The effects of donor and acceptor dopants on the fatigue behavior of bulk ceramics prepared in the manner outlined in Chapter 3 could yield interesting results about the nature of charged defects in these samples.

Secondly, electrodes could be deposited on the samples after the sample preparation (embedding in epoxy, polishing, etc.). Then the sample could be imaged in PFM, then fatigued, and finally imaged again. The resulting changes in the domain structure could yield a more detailed demonstration of the effects of fatigue on switching behavior than was shown by simply comparing virgin and fatigued samples, as was done here.